We revised the manuscript in line with the recommendations from the referees. In the following, we will list the most important modifications with respect to the ACPD version of the manuscript. A pdf manuscript compiled with LatexDiff is attached to this “Author’s Response”.

- We have carried out the trend analysis again taking into account another ENSO index and the PMM SST index. Consequently, the results have changed in large parts of the manuscript, but the major finding of our study remained unchanged.
- We have changed the colour scale from red-blue to brown-blue for all relevant figures.
- When comparing the trends from other datasets, we focus in the manuscript only on the relative (significant) TCWV trends. The comparisons of absolute trends are available in the supplement.
- We have revised the section of the trend analysis (Section 2.2) and explicitly point out the consideration of ENSO and other teleconnections. In addition, we now also show the effects of not taking teleconnections into account in the trend analysis. Appendix A has also been revised in this way.
- We address the land-ocean contrast in the RH response in Section 4.
- We point out the uncertainties in precipitation CDRs and address the relationship between SST and precipitation in Section 5.
- We have removed the section on the global TCWV response and focus instead on trends in water vapour residence time (in Section 6).

We would like to thank Kevin Trenberth for his constructive and detailed review, which helped us to identify several shortcomings in our manuscript. Below we reply to the issues raised by the referee, where
blue repeats the reviewer's comments,
black is used for our reply,
and green italics is used for modified text and new text added to the manuscript.

General comments

1. On all maps: better to use a Robinson Projection to account for convergence of meridians.

We changed the projection of all world maps to Robinson-like ("Equal Earth") projection.

2. The goals of this paper are mostly fine. Not so sure about some of the focus on trends when they are not significant! There is a lot of useful information in this paper but also some procedures and results that do not make much sense. Often the description of what was done is not very clear. Many relevant studies have preceded this, and some are referred to. A list of some others that may be of value is appended.

We regret that in some places we have not explained our procedure in a precise or comprehensible way and will remedy this in the revised version. Furthermore, we will focus on the statistically significant trends in the revised version.

3. Our understanding of TCWV is that it varies enormously with weather systems, with seasons, from land to ocean, and from year to year with ENSO. Accordingly, there is very strong natural variability, especially with phenomena such as ENSO. This is recognized in the appendix, and apparently accounted for? The local trends are often not meaningful because they simply show the phenomenological and related circulation changes. Error bars and uncertainties in trends are not always properly accounted for.

In fact, we take the effect of ENSO into account in all time series analyses in our manuscript (see also the term E in equation (4) in the discussion paper). In the revised manuscript, we also include an additional ENSO related index (TNI) and the PMM SST index in the trend analysis. In Appendix A in the discussion paper we only show how trends would look like if ENSO was not taken into account. In the revised manuscript we will move these figures into the main text and compare trends accounting and not accounting for any teleconnections along with the following text:
To highlight the influence of teleconnections on the trend results for the OMI TCWV data set, we also perform the trend analysis not accounting for them. The resulting trends and their difference are shown in Figure 3. While overall the spatial distributions of the relative trends (Fig.3a & b) look quite similar, distinct patterns emerge when looking at the trend difference Fig.3c): for instance the typical PMM and ENSO teleconnection patterns are clearly visible (e.g. dipole structure over the maritime continent in the case of ENSO). Consequently, the resulting deviations are particularly strong in the tropical and subtropical Pacific and can reach values as high as the relative trends themselves.
While we agree that local trends are affected by changes in dynamical processes, we do not find that they are not meaningful, as they can also give us an insight, albeit to be judged with caution, into the spatial distribution of changes.
We added the following text at the beginning of Section 3:

Moreover, when investigating climatological trends of TCWV on local scale, these are also influenced by changes in atmospheric dynamics and should therefore be judged with caution. Nevertheless, they can still provide us information about changes of the large-scale TCWV distribution.

Regarding the error bars and uncertainties of the trends, we think that the significant trends provide the clearest picture of changes in TCWV. However, we also believe that the occurrence of non-significant trends is also important information, as in many cases the non-significant trends have values close to zero, showing that the TCWV distribution and magnitude have changed only slightly or not at all on a long time scale. However, for the comparison of trends from different TCWV datasets, we will mainly focus on the significant trends after applying a Z and FDR test.

Over the ocean, there is a very strong relationship between SSTs and TCWV, and TCWV and precipitation, especially throughout the Tropics, see Trenberth et al 2005 and Trenberth 2011. It is never fully clear whether results include ENSO or not, or whether it was partly regressed out. It used one index to do the latter, but it is well established that at least 2 indices of ENSO are required to statistically remove ENSO (e.g. Trenberth and Stepaniak 2001). But even then, remnants will remain, and the pattern of trends shown here certainly include ENSO aspects.

Moreover, anything to do with trends should include ENSO because ENSO is part of the climate. Even if ENSO SSTs are not changing, the impacts on precipitation certainly are, and ENSO is the biggest source of droughts around the world. ENSO is part of the system, not external. It would be fine to analyze the ENSO signal separately, but this is not done. It may mean that with ENSO included the interpretation of trends in many places may change?

As mentioned above, we did not communicate clearly enough that we consider ENSO via the ONI index in our analysis. Nevertheless, we would like to thank the referee for pointing out that 2 ENSO indices should be considered in a time series analysis. We have therefore added the TNI index to our fit in addition to the ONI index and evaluated all time series once again. In addition, we tried other indices and found that the PMM SST index leads to a significant reduction in the autocorrelation of the noise in the North Pacific.

In our first analysis we did not take into account that the teleconnection indices are also subject to trends or are detrended over other time periods than ours. Therefore, we have now explicitly detrended each index again for our time period and then used these in the TCWV trend analysis.

In the revised manuscript, we added:

To account for the influence of teleconnections we include several teleconnection indices Ω in the trend analysis. For the case of ENSO, we include the NOAA Oceanic Niño Index (ONI) which according to Wagner et al. (2021) has the strongest impact on the TCWV time series distribution. Moreover, we follow the recommendations from Trenberth and Stepaniak (2001) and include a second ENSO index. In our case we apply the Trans-Niño Index (TNI; Trenberth and Stepaniak, 2001). Furthermore, we investigated the influence of several other teleconnection indices and found that the Pacific Meridional Mode (PMM) sea surface temperature index (Chiang and Vimont, 2004) has a particularly strong influence on the autocorrelation of the noise in the Pacific Ocean. Typically, trends are already removed from teleconnection indices. However, since the time series of the indices cover several decades, the detrending is optimised for this large time period. Accordingly, we have detrended the indices again for our chosen time period (2005-2020).

Overall, the consideration of TNI and PMM index as well as detrending lead to a significant reduction of TCWV trends.

4. The paper finds very little in the way of trends that are significant (Fig 2 c,d) by their tests, but their tests may be overly stringent. Given the usefulness of the dataset, it is perhaps unfortunate they chose to focus on local trends. See below.

In our significance analysis, we have tried to work as statistically "correct" as possible and avoid overstating our results, and thus also to take into account effects that are often overlooked (e.g. spatial correlation and field significance). Although this limits the amount of significant results, we can be sure that our (trend) results are highly trustworthy.

5. The issues are compounded when they analyse relative humidity involving large assumptions. The findings of changes in rh and links to precipitation are not surprising though (see Trenberth 2011). However, on land, water availability comes into play.

Following the comments about the land-ocean contrast below, we have added the following text in the section:

The reduction in relative RH over land is likely related to marked land-ocean contrast in warming, (besides various local factors such as changes in vegetation cover) (Simmons et al., 2010; Fasullo 2012): Over ocean, due to the direct link with sea surface temperature, the water vapour content can increase adequately to keep RH constant. Over land, this is usually only possible with a delay due to limited water availability, as water must first be transported there from the ocean. Since the temperature also increases much more over land than over the ocean, the decrease in RH might be due to the lack of an increased water supply from the ocean (Simmons et al., 2010).

6. L 223 on: This is mostly not correct, see Trenberth et al 2003 and Trenberth 2011, to properly account for changes in frequency and intensity, as well as amounts of precipitation. CC relates to saturation specific humidity not actual specific humidity, and one expects big differences between land and ocean. It therefore makes no sense to average globally for this and it matters how this is done. Computing relationships over land and ocean separately and then averaging (area weighting) will give different results than averaging over both land and ocean first. Also over land, it is far from clear that winter (with snow and ice) should be combined with summer.

We agree that this section is too vague. In the revised manuscript we removed this section.

Moreover, there are important differences between SST and air temperature that greatly affect these results. ERA5 has surface temperatures that would be compatible with the TCWV and surface relative humidity, but this is unlikely when a different temperature analysis (Berkeley) is introduced.

As mentioned above, this section was removed in the revised manuscript.

It is not clear what is in Fig. 7. What is the % of? Fig. 7 should be redone. L 243-244 suggests these results are flawed.

As mentioned above, the corresponding section is removed in the revised manuscript. Nevertheless, in Figure 7 we show the relative TCWV response to temperature changes (% / K), which we have determined from the relative TCWV trends (% / year) and the temperature trends (K / year):

TCWV Response = rel. TCWV trend / temperature trend.

L 260-270 and Table 1: This is very unclear, and it makes no sense to compute trends in these quantities in this way. Is ENSO included? It should be. One can compute TUT at various points and examine changes. But Table 1 makes no sense other than to say the result depends on the method.

As mentioned above, ENSO is taken into account. We followed the suggestion and calculated the TUT trends also on a local scale. Thus, we completely revised this section.

The new section is as follows:

Another key diagnostic of the hydrological cycle is the atmospheric water vapour residence time (WVRT). The WVRT can help to better understand changes in dynamic and thermodynamic processes within a changing climate (Trenberth, 1998; Gimeno et al., 2021): for instance, an increase in WVRT suggests that the length of the atmospheric moisture transport increases, i.e. the distance between moisture sink and source regions (Singh et al., 2016). Several different metrics exist for quantifying the WVRT (van der Ent and Tuinenburg, 2017; Gimeno et al., 2021), bearing in mind that the WVRT distribution or the lifetime distribution (LTD) is exponential on local scale and thus the mean value is strongly influenced by a few high values (van der Ent and Tuinenburg, 2017; Sodemann, 2020). Ideally, one would determine the LTD for each grid cell for each month from backward trajectories and then examine their changes or trends. However, this would be well beyond the scope of this paper.

Thus, for our purpose and for the sake of simplicity we focus on the so-called depletion time constant (DTC) and the turnover time (TUT). The TUT describes the global average mean age of precipitation and can be calculated as the ratio of TCWV to precipitation P:

$$TUT = \frac{\overline{TCWV}}{\bar{P}}$$

where the bar indicates global average. Typically, the TUT varies between values of 8 to 10 days and is expected to increase by 3–6% K^{-1} (Gimeno et al., 2021, and references therein). Analogously, the DTC is defined as the local ratio of TCWV to precipitation (e.g. Trenberth, 1998):

$$DTC = \frac{TCWV}{P}$$

The DTC values might vary substantially from TUT, but the global precipitation weighted average is equal to TUT (Gimeno et al., 2021).

For our investigations of trends in DTC we combine the regridded GPCP data set from Sect. 4 and the OMI TCWV data set and perform the trend analysis scheme from Sect. 2.2 to the monthly DTC values for the time range 2005 to 2020. To ensure numerical stability, we only consider monthly rain rates greater than 0.25mm d^{-1}. As a result, large parts of the subtropical oceans and deserts are excluded from the analysis.

The results of the DTC trend analyses are depicted in Figure 8. On average, we typically obtain mean DTC values between 5-10 days in the areas where rain occurs (Fig. 8a). In the subtropical dry zones, values of around 30 days and well above are found. In terms of absolute DTC trends, the most striking patterns are in the northern subtropical Atlantic with strong increases and in the northern subtropical western Pacific with strong decreases. In comparison, the distribution of relative DTC trends is much spottier, but overall, in addition to the patterns already mentioned, we obtain distinctive increases in DTC on the US west coast, in Europe, Russia and in the eastern Pacific.

For our investigations of trends in TUT we first calculate global averages of the regridded GPCP data set from Sect. 4 and the OMI and ERA5 TCWV data sets between 60°S and 60°N

for each month, then combine the time series of global averages, and finally perform the trend analysis for the TUT time series for the time range from 2005 to 2020.
Altogether, we find an increase in the global TUT for OMI and ERA5 of approximately +0.02d y^{-1} with TUT mean values of around 9.7d for OMI and 8.8d for ERA5. Combining the long-term relative trends in TUT and trends in surface air temperature, we can estimate the sensitivity of TUT to global warming r, i.e. $r = \frac{\Delta TUT}{TUT} / \Delta T$. For the case of OMI and Berkeley Earth, we find a TUT sensitivity of around 8.4%K^{-1} and for ERA5 of around 8.8%K^{-1} which is higher than the results of 3–6% K^{-1} pooled in Gimeno et al. (2021).

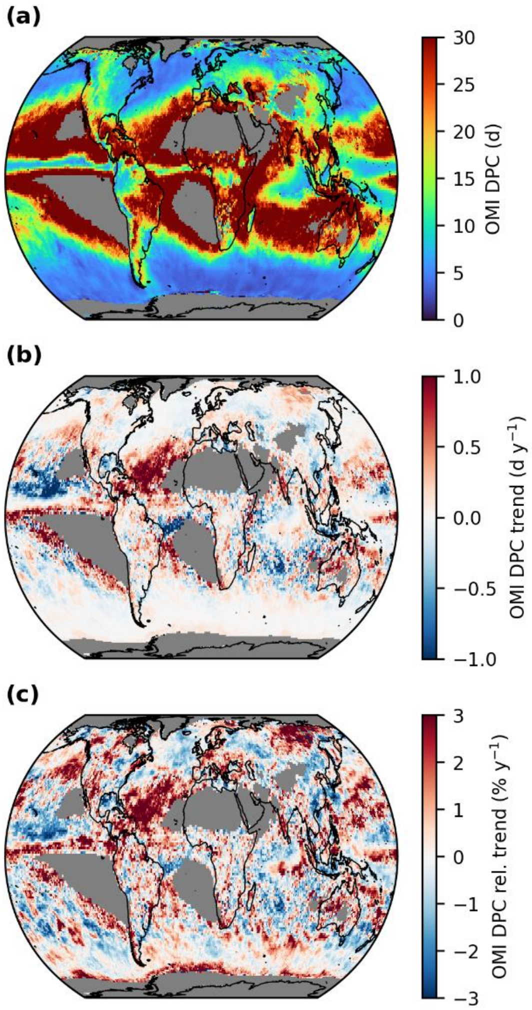

Figure 8. Global distribution of DTC trends for the time range January 2005 to December 2020. Panel (a) depicts the distribution of the mean DTC. Panels (b) and (c) depict the absolute and relative DTC trends. Grid cells for which no valid trend has been calculated are coloured grey.

Some detailed comments

L 22: The equation deals with the saturated water vapour, not just water vapour.
We added "saturated" to the sentence.

L 35-40: Wentz (2015) gives an excellent analysis of TCWV observations to that point (2015).

We added a reference to Wentz (2015).

L 48: the slowdown terminated in 2014.
We added that the slowdown terminated in 2014.

L 51: This assumption is only evoked at the surface, it clearly does not apply in the free atmosphere, e.g., where subsidence warms and dries the air.
We reformulated the sentence and explicitly mentioned that this assumption is only valid close to the surface:
[Typically, it is assumed that relative humidity] close to the surface […]

L 53 also Fasullo 2011; Simmons et al 2010.
We added the suggested references.

L 90 to 114: the accounting for persistence is not quite right or unclear. It seems a reasonable attempt though, but some rewording is warranted.

The formula in l 91 is for an AR1 process only. However, a time series with a trend will feature a strong autocorrelation at lag 1 (and 2 and 3…) In computing the AR1 value one must first remove the trend; or properly account for the higher order AR values (see Trenberth 1984). Is this what the term "residuals" means on l 97 and 107? So, the AR1 value is from N_t? ENSO also introduces persistence. In addition, the analysis assumes the variance is stationary, but this is not true because of the seasons: very different in wet vs dry seasons.
Exactly, the word "residuals" is meant to make clear that the autocorrelation used here is not that of TCWV, but of the fit "noise" or the fit "residuals" Nt. In this way, they are determined from the fit, in which the trend, seasonal components and ENSO are also taken into account. We also tested different AR processes (with lag=2, 3, 6, 12) and found only minor differences between the trend results.
In fact, the assumption of stationary variance is a limitation that could possibly be overcome by ARMA/ARIMA processes. However, the transformation of the linear equation system of the fit into this ARMA/ARIMA system is highly non-trivial (especially for unevenly spaced time series) although in the case of ARMA it is possible if the lag-1 and lag-2 coefficients of the autocorrelation function have the same sign (see e.g. Foster and Rahmstorf, 2011). However, this is not always fulfilled in our case.
Regarding the AR-model choice, we added the following text:
One limitation of the AR-model is the assumption of stationarity of the variance. Although this limitation can be overcome by using ARMA (auto-regressive moving average) or ARIMA (auto-regressive integrated moving average) processes, the determination and application of these models (for example in the transformation of the linear equation system of the fit function) is highly non-trivial, especially for the case of unevenly spaced time series. Although an ARMA(1,1) process would be possible in the case that the lag-1 and lag-2 coefficients of the autocorrelation function have the same sign (e.g. Forster and Rahmstorf, 2011), this condition is not always given in our case. Thus, we have decided to stay with the AR(1) process.
[…]
We have also tested other AR-models with lag=2, 3, 6, and 12 and found that the trend results differ only slightly from those using an AR(1) model. The corresponding trend results and the difference to the trends with the AR(1) model can be found in the supplement.

L 116 should refer to the residuals not the total fields?

Yes, this should actually refer to the residuals / "noise". We changed the sentence as follows: *... global distribution of the lag-1 autocorrelation coefficients of the fit residuals or fit noise.*

The criterion used for significance in Fig. 2c, d was 5% (line 143). It may be too harsh. The latter recognizes the spatial autocorrelation (Fig. B1) and does not take advantage of it. Line 144 and appendix B are likely misleading. L 343-4 should instead take advantage of spatial coherency to area average and remove small scale noise thereby improving signal to noise – e.g., use of 5° instead of 1° squares. Or one could lower the significance level to 10%?

We have taken up the idea of Reviewer 2 and now show all trends, significant trends (after Z-test) and "filtered" significant trends (after Z- and FDR-test) in Figure 2 in the paper (and Fig.1 in this review). Overall, a lot of trends are significant at 5%, so we do not think that our criteria are too strict (see Fig. 1c and 1d). Regarding 5° vs. 1° resolution, we found almost no differences in the distribution of significant trends, but obviously some information is lost due to the poorer resolution (compare Fig.1 vs. Fig.2). Therefore, we continue to stick with 1° x 1° resolution.

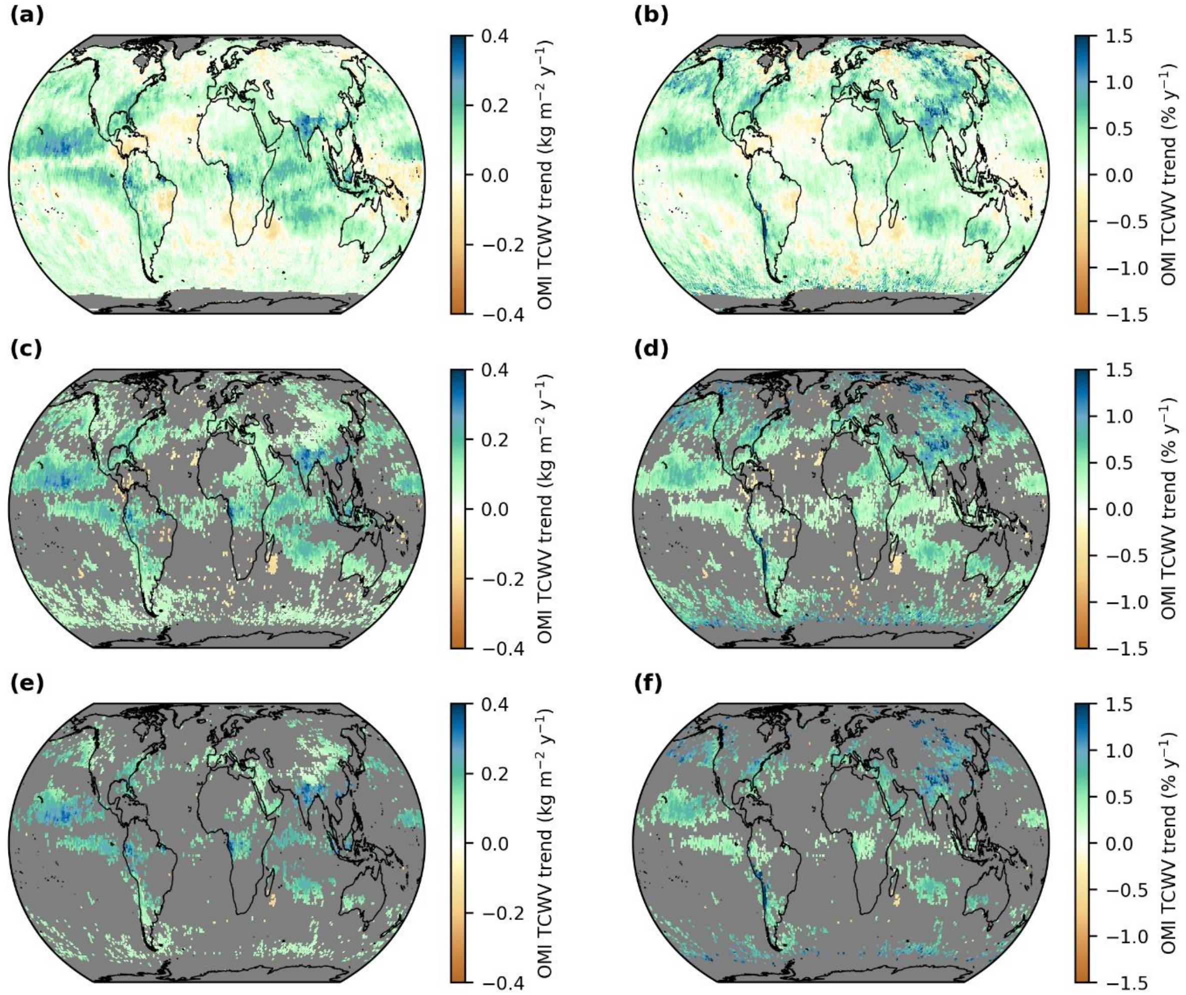

Fig.1: Global distribution of TCWV trends derived from the MPIC OMI TCWV data set. Panels (a) and (b) depict the calculated absolute and relative TCWV trends, respectively. Panels (c) and (d) depict the remaining significant trends after the application of the Z-test. Panels (e) and (f) depicts the remaining significant trends after the application of the Z-test and the FDR test.

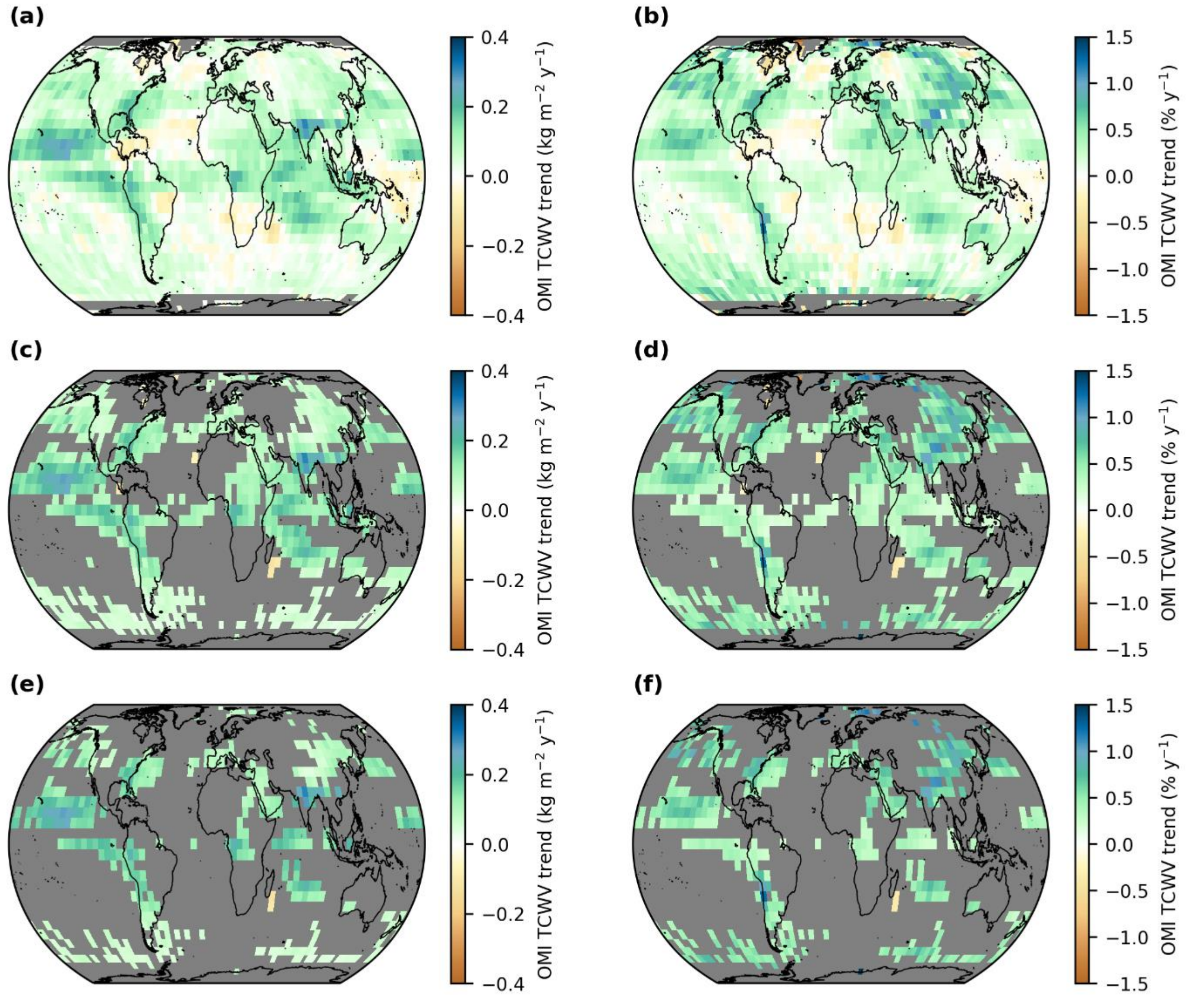

Fig.2: Same as Fig.1, but with 5° x 5° resolution.

L 137-8: the overall pattern of change is one that surely aliases ENSO to some degree (the coherence of the SPCZ and ITCZ changes), see Fig, A1. Removal of ENSO should use at least 2 indices. However, ENSO is real, and changes in humidity and precipitation with ENSO are also a climate signal (one expects larger values for same index value).

We followed your recommendations and included 2 (detrended) ENSO indices (ONI & TNI) as well as the PMM SST index in the new analysis. But since "ENSO is real and changes … with ENSO are also a climate signal", we also include trends on the actual measurements without including ENSO indices in the trend analysis.

L 156: Given the lack of significant trends in Fig. 2, why is there a focus on trends now? The comparison between Figs 3 and 4 highlights the dependence on data period.

As we work as statistically cleanly as possible (and thereby avoid overinterpreting irrelevant or insignificant trends) we consider the remaining significant trends to be real and worth reporting. Actual numbers of course depend on the considered data period, and of course the trend results become more meaningful for longer time periods. Thus, we make use of our new H2O product for OMI, which provides the longest single-instrument time series for this type of measurements. Hence, we are confident that – in spite of all limitations – showing trends is an important information for the reader.

L 177: section 4 should refer to Simmons et al. (2010) and Fasullo (2011). Land vs ocean must be better recognized.
We incorporated the papers by Fasullo (2011) and Simmons et al. (2010) (see comment above).

L 201-214 should account for above studies and also changes in salinity, which better deals with the DDWW aspects: Cheng et al 2020.
We added the following text:
In addition, other studies show that changes in precipitation correlate very well with changes in ocean salinity, suggesting a "fresh gets fresher, salty gets saltier" pattern (Cheng et al., 2020, and references therein).

L 220-220: the discussion related to Fig 6, needs to better account for the changes in SSTs, see Trenberth 2011.
We added the following text:
Trenberth (2011) and Trenberth and Shea (2005) analysed local correlations between precipitation and surface temperature for cold and warm seasons and reported mainly positive correlations over ocean and negative correlations year round over land throughout the tropics. However, over ocean the correlations also depend on whether the (sea) surface temperature is driven by the ocean or by the atmosphere (Trenberth and Shea, 2005). While in some regions of the subtropics we can also find this high correlation in the trend patterns of precipitation and surface temperature (e.g. increase in precipitation in the northern subtropics in the eastern Pacific or decrease in the subtropical Atlantic over ocean; decrease in Brazil or South Africa over land), we cannot find a direct link for the striking negative precipitation trends in the equatorial Pacific. However, it should also be taken into account that a large part of the precipitation trends are not statistically significant.

L 223 on: This is mostly not correct, see Trenberth et al 2003 and Trenberth 2011, to properly account for changes in frequency and intensity, as well as amounts of precipitation. CC relates to saturation specific humidity not actual specific humidity, and one expects big differences between land and ocean because of water availability. It makes little sense to average globally for this. Moreover, there are important differences between SST and air temperature that greatly affect these results. It is not clear what is in Fig. 7? What is the % of? Also over land, it is far from clear that winter (with snow and ice) should be combined with summer. Fig. 7 should perhaps be redone. L 243-244 suggests these results are flawed?
The corresponding section has been removed in the revised manuscript.

L 245: The residence time is a reasonable concept and relates to the amount vs flux out.

L 260-270: Table 1. What are T trends here: not 0.02: has to be 0.02 per year? Same for all here: per year? There are no error bars on any of these estimates; for instance, global precipitation trends are not significant. The main precipitation fluctuations are associated with ENSO. There also remain uncertainties in precipitation (e.g. Prat et al. 2021) – and several other papers in same issue. It would be better for most readers to see the values of TUT, not the trends. TUT trends in % make no sense. It is also not clear why global temperatures enter this discussion. Suggest the authors focus more on the actual values instead of uncertain trends, although decadal changes may warrant mention?

We have revised the TUT section and now distinguish between local trends in the residence time (more precisely the depletion time constant) and trends in the globally averaged residence time (TUT).

In addition, we addressed the uncertainties in the rainfall data sets. According to Prat et al. (2021), however, "For accumulation periods greater than the day (i.e., week, month, years), all SPPs perform satisfyingly, which makes them suitable for long term hydro-logical and hydroclimatological applications." However, it should also be taken into account that Prat et al. (2021) used GPCPv2, whereas we use the latest GPCP version (v3.2).

Although precipitation climate data records (CDRs) allow a global analysis, they are subject to large uncertainties, as satellite and rain-gauge observations do not have good spatio-temporal coverage, weak and short rain events are not well detected or even missed and satellite retrievals can determine the rain rate only indirectly. Thus, deviations of about 50% in the daily rain rate can occur compared to in situ measurements (e.g. Prat et al., 2021). Nevertheless, Prat et al. (2021) show that over accumulation periods of month or years, precipitation CDRs perform satisfactorily. Moreover, Prat et al. (2021) used an older GPCP version (v2) than ours in their evaluation study.

Similarly in Fig D1, no errors bars are included or areas where trends are not significant indicated.

We have revised figure D1 and now added the maps of significant trends.

References

Cheng, L., K. E. Trenberth, N. Gruber, J. P. Abraham, J. Fasullo, G. Li, M. E. Mann, X. Zhao, and J. Zhu, 2020: Improved estimates of changes in upper ocean salinity and the hydrological cycle. *J. Climate*, **33**, 10357-10381

Fasullo, J. 2011. A mechanism for land–ocean contrasts in global monsoon trends in a warming climate. Clim Dyn. DOI 10.1007/s00382-011-1270-3

Excerpt from abstract

"A feedback mechanism is proposed rooted in the facts that land areas warm disproportionately relative to ocean, and onshore flow is the chief source of monsoonal moisture. Reductions in lower tropospheric relative humidity over land domains are therefore inevitable and these have direct consequences for the monsoonal convective environment including an increase in the lifting condensation level and a shift in the distribution of convection generally towards less frequent and potentially more intense events."

Prat, O. P., et al. 2021: Global Evaluation of Gridded Satellite Precipitation Products from the NOAA Climate Data Record Program. J Hydromet. 22, 2291-2310.

Simmons, A. J., K. M. Willett, P. D. Jones, P. W. Thorne, and D. P. Dee (2010), Low-frequency variations in surface atmospheric humidity, temperature, and precipitation: Inferences from reanalyses and monthly gridded observational data sets. J. Geophys. Res., 115, D01110, doi:10.1029/2009JD012442.

Trenberth, K. E., 1984: Some effects of finite sample size and persistence on meteorological statistics. Pt. I: Autocorrelations. *Mon. Wea. Rev.*, **112**, 2359–2368.

Trenberth, K. E., 2011: Changes in precipitation with climate change. Climate Research, 47, 123-138, doi: 10.3354/cr00953

Trenberth, K. E., and D. P. Stepaniak, 2001: Indices of El Niño evolution. *J. Climate*, **14**, 1697–1701.

Trenberth, K. E., A. Dai, R. M. Rasmussen and D. B. Parsons, 2003: The changing character of precipitation. *Bull. Amer. Meteor. Soc.*, **84**, 1205-1217.

Wentz, F. J. 2015: A 17-Yr Climate Record of Environmental Parameters Derived from the Tropical Rainfall Measuring Mission (TRMM) Microwave Imager. J Climate, 28, 6882-6902. DOI: 10.1175/JCLI-D-15-0155.1

We would like to thank Chunlüe Zhou for his constructive and detailed review. Below we reply to the issues raised by the referee, where
blue repeats the reviewer's comments,
black is used for our reply,
and green italics is used for modified text and new text added to the manuscript.

The authors investigated trends in total column water vapor (TCWV) measured by the Ozone Monitoring Instrument (OMI) from 2005 to 2020, and combined air temperature to discuss changes in relative humidity and associated TCWV response to global warming. This is a hot topic in our climate change community, and this study might add some values to the topic. The logic of the manuscript is overall good, but still lacks sufficient discussions with previous studies and also many details, for instances, readers would not know what period of the trend in Figure 3 when they do not read your main text. I think it deserves to be published on ACP after a major revision.
Thanks for pointing out this issue. We added information about the time period of the trend analysis to the title of the respective figures.

Below I made a summary of my main concerns as they pervade the manuscript. Hope they can help improve the quality of manuscript.

First, the most important question is about possible impact of climate variability on trend estimate. For a short data period (about 15 years), climate variability such as ENSO might dominate the estimated trend. ENSO has diverse impacts on TCWV, so even though the authors removed the ENSO impact by a regression, it is unclear whether that is sufficient. In particular, a regression was done over a short period.
We agree with the referee that it would be desirable to have as long a time series as possible and that 16 years are rather short on climatological scales. However, we would like to emphasise that previous TCWV studies have used similarly short or even shorter time periods. Furthermore, our TCWV data have been obtained from only one instrument and not compiled from different instruments. While this restricts our analysis to the time period of the instrument, one advantage is, for example, that we do not have to consider inter-instrumental offsets.
In the (revised) manuscript we wrote:
[The major advantages of this TCWV data set in comparison to others are that on the one hand the data set provides a consistent time series since it is based on measurements from only one satellite instrument]. Thus, inter-instrumental offsets do not have to be corrected when merging the data time series of the different instruments. [On the other hand, in contrast to other spectral ranges, TCWV retrievals in the visible "blue" spectral range have a similar sensitivity over ocean and land surfaces and thus allow for consistent global analyses.]
Regarding ENSO, the other Referee (Kevin Trenberth) pointed out to us that at least 2 ENSO indices should be considered in the analysis, which we also implemented in the results of the revised version. Thus, we believe that we have not completely eliminated the influence of ENSO on trend, but at least reduced it as much as possible.
In the revised manuscript, we include both: an analysis based on the original data as is, and an analysis including two dominant ENSO indices. The results differ, as expected, but the overall conclusion is not affected.

Second, if directly considering them like Yt = m+ b·Xt +St +Yt-1 +Nt where Yt-1 should include the impacts of ENSO and autocorrelation, what is different from the result of Equation 4? Will be better?

Thank you for this idea! We have tried this “new” approach and the results are shown in the graph below (together with our “traditional” approach). While at first glance the results look quite similar, a closer look reveals a weak dipole structure over the maritime continent in the “new approach” in comparison to the “traditional” results.

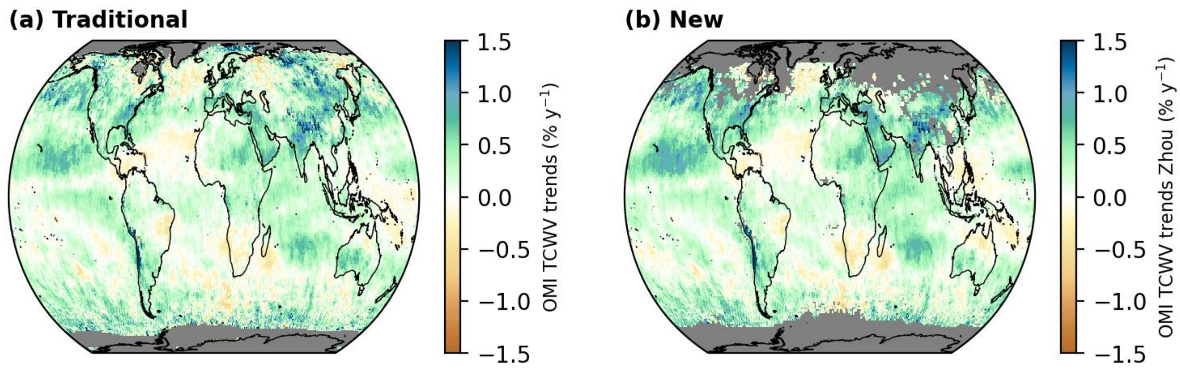

This ENSO-like patterns become clearly visible when we take the difference of the trends, and have a comparable structure as in Figure A1, in which we demonstrated the effect of neglecting the influence of ENSO on the TCWV trends.

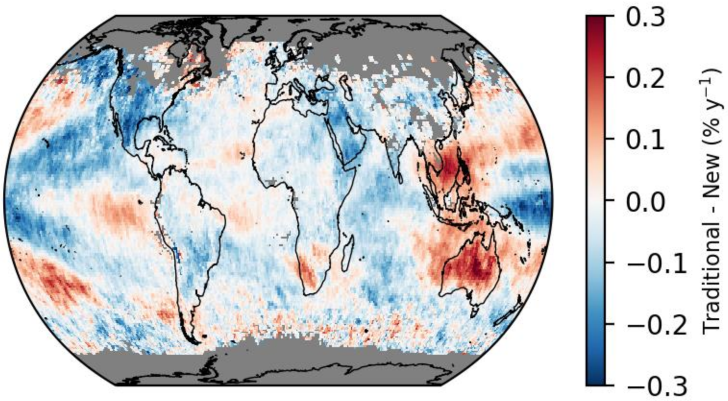

Even though it might be worthwhile to include ENSO in the analysis of this "new" approach, this would “contradict” its initial idea, we conclude that it is better to stay with our previous approach.

Regarding Equation (4), we would like to point out that it is not a matter of reducing the autocorrelation of Yt, but of the fit residuals or the fit noise Nt. If we did not take the autocorrelation in Nt into account, our significance tests would give us misleading results (see also the beginning of Section 2.2 and Weatherhead et al. (1998)).

Second, about data: The wettest spots locate in India (Fig. 3a vs 3b or all the other figures including Fig. 5), and my main concern is why? Is it related to satellite retrievals? In my recent paper, Zhou et al., (2021), it’s found that radiosonde temperature data quality is quite low in India which seriously worsens trend estimate. Is the similar case for OMI TCWV? More relevant reasons will be discussed.

With the inclusion of the TNI and the PMM index in the analysis and the detrending of the teleconnection indices, the trend values have decreased overall, so that in India the values are approximately similar to those over the subtropical ocean. The extraordinarily high values in the Himalayas are probably rather artefacts of the satellite retrieval, as this also depends on surface parameters such as the height above sea level and the albedo. Therefore, similarly high values can also be seen in the Andes region. On the other hand, we have not been able to detect any trends in surface albedo (see also panel (c) in Figure C2).
Thus, we added the following text to the revised manuscript:
We also obtained distinctively high trend values over mountains such as the Himalayas and Andes. However, these high values are likely artefacts due to uncertainties of the satellite retrieval, for example in the input data for the ground elevation. Thus, we decided to filter these artefacts and only show grid cells for which the mean ground elevation is lower than 3000m above mean sea level based on the GMTED2010 elevation data set (Danielson and Gesch, 2011).

Third, about ERA5 and GOME (line 161-164, 167-168): What TCWV products were assimilated in ERA5? Zhou et al., (2018) compared near-surface water vapor pressure trends from the current reanalysis and observation, and some information there can help better show their differences. There are many differences between OMI and GOME, especially in India, North America, Northeast Asia and Europe (Fig. 4). Good to show some statistics about the relationship of OMI and ERA5/GOME? Such as spatial correlation, RMSE? OR show their difference map against OMI? More simple comparisons should be provided rather than only a conclusion.
To our best knowledge, no (satellite) TCWV products are directly assimilated into ERA5, but typically the Brightness Temperature of microwave and infrared instruments and the ZPD of GPS-RO instruments (besides the in-situ measurements of radiosonde data, etc.). See also section 5 in the ERA5 paper by Hersbach et al. (2020).
A detailed analysis of the OMI dataset with comparisons to ERA5 (and also SSM/I and the ESA WV CCI dataset) can be found in Borger et al. (2021a) (doi:10.5194/essd-2021-3, currently under discussion). Therefore, we have refrained from a comparison to ERA5 here.
We reformulated the following text to Section 2.1:
In an extensive validation study, Borger et al. (2021a) showed that the data set is in good overall agreement to other reference data sets such as the satellite data from RSS SSM/I (Mears et al., 2015; Wentz, 2015) or the reanalysis model ERA5 (Hersbach et al., 2019), especially over ocean surface.

Fourth, about TCWS responses to air temperature: The authors estimated a larger response than the theoretical value, i.e., 7%. I think it’s rather reasonable on local or regional scale, because the response on local or regional scale is not only thermodynamic but also dynamical. Zhou et al., (2017) isolated the responses of precipitation to long-term changes and short-term variations in air temperature and showed a much larger response than 7%. More details and discussions can be seen in that paper, and some discussion about possible impacts of short data period, and thermodynamic versus dynamic contributions will be revised into the manuscript.
Many thanks for this hint and the valuable suggestions! However, after reviewer #1's (Kevin Trenberth) assessment, we have decided not to include this section in the revised version.

Finally, about figure: There are several repeated subfigures. I think the authors should keep only % subfigures and remove subfigures for absolute values. Because the latter do not

provide additional information. Is Figure 2a-2b the same as Figure 2a and 2c? It would be better if using blue for wet and red for dry in colorbar.
We have changed the colour bar in all relevant figures from red-blue to brown-blue. Furthermore, when comparing trends between the different datasets, we only focus on relative trends. The absolute trends are made available in the Supplement Section.

Specific comments:
1. Not good to use an abbreviation in Title
Since satellite instruments are mostly known by their acronym (e.g. IASI, SSM/I, MHS, AIRS, MODIS), we would like to stick with the abbreviation in the title.

2. Why not plot directly the autocorrelation values in Figure 1? The sign of autocorrelation also has scientific meaning.
We have adjusted Figure 1 and now also show negative values.

3. Lines 147-149, Figure 2c-2d still show many sparse dots even after applying the FDR test. Could show both results of the Z-test and FDR test?
We have adapted Figure 2 and now show the significant trends in addition to all trends and the FDR trends.

4. Lines 152-153, 'increasing or decreasing H2O absorption' is the same as 'changing atmospheric water vapour content', so change to 'changing saturated water vapour content'?
"changing saturated water vapour content" would imply that the relative humidity would remain constant. Since we find in our work that this is not the case (on local scales), we would therefore stick with "changing atmospheric water content".

5. Line 215, pay more attention to North America and India as comparing RH in Figure 6.
We rewrote the relevant paragraph as follows:
Figure 7 depicts the obtained trends in precipitation as well as the relative RH trends from OMI. Comparing the trend distributions of the monthly mean rain rates to the relative RH trends, negative and positive trends in precipitation and RH match quite well over the tropical and subtropical ocean, especially over the tropical Pacific and the Northern subtropical Atlantic. While over land within the subtropics an acceptable match can be determined in some regions (e.g. South Africa, Brazil), the patterns of the relative RH and rain rate trends no longer match well towards mid and high latitudes (e.g. in North America), likely because in these regions the rain rate is mainly determined by atmospheric dynamics (cyclone or storm tracks) rather than thermodynamics. Furthermore, the distinctive increases of relative RH in the mountainous regions of South America (Andes) and northern India (Himalayas) are likely due to the inadequacies in the OMI TCWV satellite data caused by the complex topography (see also Sect. 3.1.).

6. Lines 131-132, half is not enough, especially for a short period. I recommend some 80 or 90%.
The OMI TCWV retrieval depends on the annual cycle of the solar zenith angle and is only applied over snow/ice-free surfaces, which is why complete coverage is not possible during the winter months, especially at higher latitudes. Thus, for some of these regions, 3-4 months per year are missing. An 80% or 90% filter would therefore remove these regions. Since these regions are particularly interesting for climate studies, we would like to keep them. Instead, we provided a map with temporal coverage in the Supplement/Appendix and

mention at appropriate places in the manuscript (including figure captions) that the values in the high latitudes should be interpreted with caution due to incomplete temporal coverage. We added the following text to Section 3:

At this point, we would like to note that, especially in the high latitudes, complete temporal coverage within the MPIC OMI TCWV data set is not always given. For example, the winter months are often missing because no satellite measurements are available due to the seasonal solar cycle or ice cover. Thus, the trends shown are not representative for the entire year, but only for part of it, and should be interpreted with caution. However, we would still like to present the results, as these regions are of great interest in climate research. A map of the fractional temporal coverage is provided in Fig. S1 in the supplement.

References:

Zhou, C., Wang, J., Dai, A. & Thorne, P. W. A new approach to homogenize global sub-daily radiosonde temperature data from 1958 to 2018. J. Clim. 34, 1163-1183 (2021).

Zhou, C., He, Y. & Wang, K. On the suitability of current atmospheric reanalyses for regional warming studies over China. Atmos. Chem. Phys. 18, 8113-8136, doi:10.5194/acp-2017-966 (2018).

Zhou, C. & Wang, K. Quantifying the sensitivity of precipitation to the long-term warming trend and interannual-decadal variation of surface air temperature over China. J. Clim. 30, 3687-3703, doi:10.1175/jcli-d-16-0515.1 (2017).

Analysis of global trends of total column water vapour from multiple years of OMI observations

Christian Borger, Steffen Beirle, and Thomas Wagner

Satellite Remote Sensing Group, Max Planck Institute for Chemistry, Mainz, Germany

Correspondence: Christian Borger (christian.borger@mpic.de) and Thomas Wagner (thomas.wagner@mpic.de)

Abstract. In this study, we investigate trends in total column water vapour (TCWV) retrieved from measurements of the Ozone Monitoring Instrument (OMI) for the time range between January 2005 to December 2020. The trend analysis reveals on global average an annual increase in the TCWV amount of approximately $+0.056\,\mathrm{kg\,m^{-2}\,y^{-1}}$ or $+0.24\,\%\,\mathrm{y^{-1}}$ $+0.054\,\mathrm{kg\,m^{-2}\,y^{-1}}$ or $+0.21\,\%\,\mathrm{y^{-1}}$. After the application of a Z-test (to the significance level of 5%) and a false discovery rate test to the results of the trend analysis, mainly positive trends remain, in particular over the Northern subtropics in the East Pacific.

Combining the relative TCWV trends with trends in air temperature, we also analyze trends in relative humidity (RH) on local scale. This analysis reveals that the assumption of temporally invariant RH is not always fulfilled: we obtain increasing and decreasing RH trends over large areas of the ocean and land surface and also observe that these trends are not limited to arid and humid regions, respectively. For instance, we find decreasing RH trends over the (humid) tropical Pacific ocean in the region of the intertropical convergence zone. Interestingly, these decreasing RH trends in the tropical Pacific ocean coincide well to decreasing trends in precipitation.

Additional investigations of the global response of TCWV to changes in (surface) air temperature show that the relative TCWV trends do not follow a Clausius-Clapeyron response (i.e. 6–7 $\%\,\mathrm{K^{-1}}$) and are about 2 to 3 times higher even for the case of global averages. Moreover, by combining the trends of TCWV, surface temperature, and precipitation we derive trends for the global water vapour turnover time (TUT) of approximately $+0.02\,\mathrm{d\,y^{-1}}$. Also, we obtain a TUT rate of change of around $11\,\%\,\mathrm{K^{-1}}$ $8.4\,\%\,\mathrm{K^{-1}}$ which is 2 to 4 3 times higher than the values obtained in previous studies.

1 Introduction

Water vapour is the most abundant greenhouse gas in the Earth's atmosphere and is involved in several atmospheric processes across all atmospheric scales: starting from phenomena like cloud droplet growth on the microscale, to thunderstorms on the mesoscale, to hurricanes on the synoptic scale and finally on the climate or global scale by influencing the Earth's energy balance via the greenhouse effect and cloud, lapse rate, and water vapour feedback mechanisms (Kiehl and Trenberth, 1997; Randall et al., 2007). According to the Clausius-Clapeyron (CC) equation changes in saturated water vapour are closely linked to changes in air temperature:

$$\frac{dE}{E} = \frac{L_v(T)}{R_v}\frac{dT}{T^2} \tag{1}$$

with saturation water vapour pressure E, latent heat of vaporization L_v, the specific heat capacity of water vapour R_v, and the air temperature T. For typical atmospheric conditions the CC-equation yields that for a temperature increase of 1 K it can be expected that the water vapour concentration increases by approximately 6-7% if relative humidity remains unchanged (Held and Soden, 2000). Thus, given its key role in many atmospheric processes and considering the global warming of the atmosphere and ocean within the last decades, accurate monitoring of changes of the global water vapour distribution is essential not only for a better understanding of the Earth's hydrological cycle, but also of the climate system in general.

Several quantities exist to characterise the content of water vapour in the atmosphere. To determine the distribution of these quantities on global scale, satellite missions offer great opportunities. Depending on the spectral range, satellite instruments can provide different information: for example, in the radio and thermal infrared spectral range it is possible to retrieve information of the vertical profile of the water vapour concentration (e.g. Kursinski et al., 1997; Susskind et al., 2003). Another important quantity is the water vapour content integrated over the complete atmospheric column, also known as "integrated water vapour" or "total column water vapour" (TCWV). In addition to the spectral ranges already mentioned, this quantity can be retrieved in the microwave (Rosenkranz, 2001)(Rosenkranz, 2001; Wentz, 2015), in the shortwave- and near-infrared (Bennartz and Fischer, 2001; Gao and Kaufman, 2003), and in the visible spectral range (e.g. Noël et al., 1999; Lang et al., 2003; Wagner et al., 2003; Grossi et al., 2015; Borger et al., 2020).

Based on these satellite observations, several studies in the past have investigated trends or changes in the global water vapour distribution (e.g. Trenberth et al., 2005; Wagner et al., 2006; Mieruch et al., 2008; Wang et al., 2016) and found rates of change that correspond to the CC-response (e.g. Trenberth et al., 2005). Trenberth et al. (2005) analyzed trends for the time period of 1988 to 2003 from a TCWV data set of merged microwave satellite sensors and found generally positive trends that are consistent with assumption of fairly constant relative humidity. Mieruch et al. (2008) combined TCWV measurements from GOME and SCIAMACHY in the visible red spectral range and determined also positive TCWV trends for the time period January 1996 to December 2003. More recently, Wang et al. (2016) investigated TCWV trends for the time period from 1995 to 2011 for a TCWV data set combining measurements from radiosondes, GPS radio occultation, and microwave satellite instruments. They found positive but slightly weaker TCWV trends which they attributed to the slowdown in the global warming rate since 2000. 2000 that terminated in 2014.

Nevertheless, a major limitation of the assumption of a CC-response is the assumption of temporally invariant relative humidity. Typically, it is assumed that the relative humidity close to the surface (especially over the ocean) remains constant, which was also confirmed by Dai (2006). Over land surfaces, however, this assumption is not always given : (Simmons et al., 2010; Fasullo, 2012): for instance Dunn et al. (2017) showed with their observational data, first a constant, and then a clear decrease in near-surface relative humidity over land masses since 2000.

In this study, we continue the analysis of the trends in TCWV. For this purpose, we are using an observational TCWV data set (Borger et al., 2021a) based on measurements of the Ozone Monitoring Instrument (OMI; Levelt et al., 2006, 2018) in the visible blue spectral range. In doing so, we investigate not only how strong the trends in water vapour are on local scale, but also to what extent the assumption of constant relative humidity is fulfilled there. Moreover, we also investigate how sensitive the global atmospheric water cycle (more specifically the TCWV and water vapour residence time) responds to changes in surface air temperature.

For this purpose, the paper is structured as follows: in Sect. 2 we briefly introduce the OMI TCWV data set and detailedly describe the scheme for the trend analysis. Then, in Sect. 3 we present the trend results from the OMI TCWV data set and put these results in context to the trend results from other data sets. In Sect. 4 we analyze local trends in relative humidity derived from the OMI TCWV trends and investigate how these are related to changes in precipitation in Section 5. Moreover, in Sect. ?? 6 we analyze the responses of the global atmospheric water cycle water vapour residence time to global warming. Finally, in Sect. 7 we will briefly summarize our results and draw conclusions.

2 Data set and methodology

2.1 MPIC OMI TCWV data set

For our study, we use the monthly mean MPIC OMI TCWV data set from Borger et al. (2021a, b). The data set is based on measurements of the Ozone Monitoring Instrument OMI (Levelt et al., 2006, 2018) which are analyzed by means of Differential Optical Absorption Spectroscopy (DOAS; Platt and Stutz, 2008) in the visible blue spectral range using the TROPOMI TCWV retrieval of Borger et al. (2020): First, a spectral analysis is performed in a fit window of 430–450 nm taking into account the specific instrumental properties of OMI (more details in Borger et al., 2021a). Then, these fit results are converted to TCWV via an iterative algorithm finding the optimal water vapour profile shape.

The data set covers the time period January 2005 to December 2020 and provides the TCWV values on a spatial resolution of $1^\circ \times 1^\circ$. In an extensive validation study, Borger et al. (2021a) showed that the data set is in good overall agreement to other reference data sets such as RSS SSM/I (Mears et al., 2015; Wentz, 2015) or ERA5 (Hersbach et al., 2020), especially over ocean surface. Moreover, Borger et al. (2021a) demonstrated in a temporal stability analysis that their data set is consistent with the temporal changes of the reference data sets and that it shows no significant deviation trends (i.e. relative deviation trends smaller than 1% per decade) which is particularly important for climate studies.

The major advantages of this TCWV data set in comparison to others are that on the one hand the data set provides a consistent time series since it is based on measurements from only one satellite instrument. Thus, inter-instrumental offsets do not have to be corrected when merging the data time series of the different instruments. On the other hand, in contrast to other spectral ranges, TCWV retrievals in the visible "blue" spectral range have a similar sensitivity over ocean and land surfaces and thus allow for consistent global analyses.

2.2 Trend analysis

For the trend analysis we follow the approaches of Weatherhead et al. (1998), Mieruch et al. (2008), and Schröder et al. (2016) in which the fit function is given as:

$$Y_t = m + b \cdot X_t + S_t + \Theta_t + N_t = \mathbf{M_t} x + N_t \tag{2}$$

with the intercept m, the slope or trend b respectively, the increasing time index X_t, the seasonal components S_t, and a component accounting for the influence of geophysical teleconnections (e.g., the El Niño / Southern Oscillation, ENSO) Θ_t, which can all be summarized in a matrix $\mathbf{M_t}$. The term N_t stands for the fit residuals with respect to the measurement time series.

The seasonal components are modelled as a sum of sine and cosine functions with up to 4 frequencies:

$$\mathsf{S_t} = \sum_{\mathsf{i}=1}^{4} [\mathsf{c_i} \sin(\mathsf{i} \cdot \omega \mathsf{X_t}) + \mathsf{d_i} \cos(\mathsf{i} \cdot \omega \mathsf{X_t})] \tag{3}$$

with $\omega = \frac{2\pi}{12}$.

To account for the influence of teleconnections we include several teleconnection indices Ω_i in the trend analysis. For the case of ENSO we include the NOAA Oceanic Niño Index (ONI) which according to Wagner et al. (2021) has the strongest impact on the TCWV time series distribution. Moreover, we follow the recommendations from Trenberth and Stepaniak (2001) and include a second ENSO index. In our case we apply the Trans-Niño Index (TNI; Trenberth and Stepaniak, 2001). Furthermore, we investigated the influence of several other teleconnection indices and found that the Pacific Meridional Mode (PMM) sea surface temperature index (Chiang and Vimont, 2004) has a particularly strong influence on the autocorrelation of the noise in the Pacific ocean. Typically, trends are already removed from teleconnection indices. However, since the time series of the indices cover several decades, the detrending is optimised for this large time period. Accordingly, we have detrended the indices again for our chosen time period (2005-2020). Apart from the 3 detrended index time series themselves, also their derivatives are considered within the trend analysis:

$$\Theta_{\mathsf{t}} = \sum_{\mathsf{i}=1}^{3} \theta_{1,\mathsf{i}} \cdot \Omega_{\mathsf{i}} + \theta_{2,\mathsf{i}} \cdot \frac{\partial \Omega_{\mathsf{i}}}{\partial \mathsf{t}} \tag{4}$$

For the fit residuals N_t we assume that they follow a first-order autoregressive process AR(1), which can be described as:

$$\mathsf{N_t} = \phi \mathsf{N_{t-1}} + \varepsilon_{\mathsf{t}} \tag{5}$$

with the autocorrelation ϕ. In classical statistical methods it is often assumed that data are independent. However, this is not always the case in environmental data, in particular for time series analysis, in which data are likely temporally autocorrelated. Not Thus, not accounting for autocorrelation can give misleading results when these classical statistical test methods are applied to strongly persistent time series (Wilks, 2011). If the residuals N_t follow a first-order autoregressive process (AR(1)) with autocorrelation ϕ:

$$N_t = \phi N_{t-1} + \varepsilon_t$$

(von Storch, 1999; Wilks, 2011). For instance, Weatherhead et al. (1998) showed that in the presence of temporal autocorrelation the uncertainty of a linear trend is linked to the level of autocorrelation as:

$$\sigma_{trend}^2 \propto \sigma_N^2 \cdot \frac{1+\phi}{1-\phi} \propto \frac{\sigma_\varepsilon^2}{1-\phi^2} \cdot \frac{1+\phi}{1-\phi} \tag{6}$$

with the fit error σ_N^2 influenced by the autocorrelation and the "true" fit error σ_ε^2. Consequently, positive (negative) autocorrelation can lead to an underestimation (overestimation) of the uncertainty of the trend which in turn can cause misleading results when classical statistical test methods (e.g. Z-test) are used to classify if a trend is significant or not. Moreover, as the fit is not statistically efficient (i.e. it does not have the minimal variance), also the fit results can deviate from the "truth" (see also Appendix A).

ThusHence, to account for the autocorrelation of the fit residuals within the trend analysis, we follow the approaches of Weatherhead et al. (1998), Mieruch et al. (2008), and Schröder et al. (2016) and assume that the residuals can be described by a first-order autoregressive process AR(1). The fit function is then given as :

$$Y_t = m + b \cdot X_t + S_t + E_t + N_t = \mathbf{M_t}x + N_t$$

with the intercept m, the slope or trend b respectively, the increasing time index X_t, the seasonal components S_t, a component accounting for the influence of the El Niño / Southern Oscillation (ENSO) E_t, and the residuals N_t. The seasonal components are modelled as a sum of sine and cosine functions with up to 4 frequencies:

$$S_t = \sum_{i=1}^{4} [c_i \sin(i \cdot \omega X_t) + d_i \cos(i \cdot \omega X_t)]$$

with $\omega = \frac{2\pi}{12}$. For the ENSO components we use the NOAA Oceanic Niño index (ONI) Ω which according to Wagner et al. (2021) has the strongest impact on the TCWV time series distribution. Apart from the index time series itself, also its derivative is considered within the analysis:

$$E_t = e_1 \cdot \Omega + e_2 \cdot \frac{\partial \Omega}{\partial t}$$

To effect of autocorrelation, we use the Prais-Winsten transformation (Prais and Winsten, 1954) and proceed as follows: First, to calculate the autocorrelation ϕ of the residuals, we perform a linear least-squares fit of Eq. (2) to the time series of the TCWV data set as first guess for each gridcell which yields the time series of N_t. Then, we estimate the autocorrelation function using the gaussian-kernel-based cross-correlation function algorithm as described in Rehfeld et al. (2011) via the NEST package (http://tocsy.pik-potsdam.de/nest.php, last access: 15 Feb 7 June 2022). The advantage of this algorithm is that it takes into account the complete data of an irregular spaced time series. From the autocorrelation function the lag-1 autocorrelation ϕ can then be derived by simple linear algebra.

Figure 1 illustrates the global distribution of the absolute values of the lag-1 autocorrelation coefficient coefficients of the fit residuals from the trend analysis of the OMI TCWV data set. Distinctive patterns of enhanced autocorrelation are observable within the tropics and subtropics, in particular in the Southern Pacific ocean with values reaching up to about 0.5. Towards higher latitudes the distribution of the autocorrelation becomes spottier and the values decrease to about 0.

After the calculation of the autocorrelation for each gridcell the AR(1)-model can be prepared via the transformation matrix

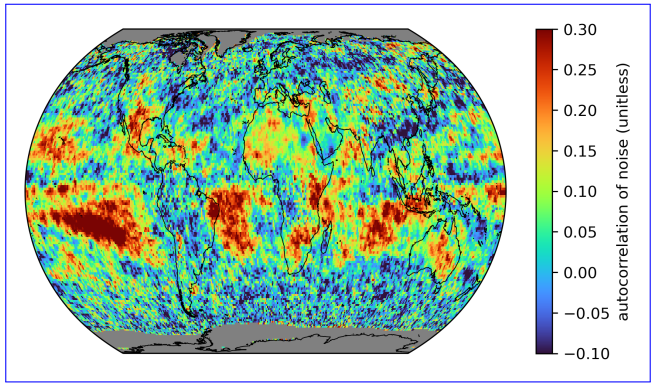

Figure 1. Global distribution of the absolute values of the lag-1 autocorrelation coefficients of the fit residuals (or fit noise) of the trend analysis for the MPIC OMI TCWV data set.

$\mathbf{P}$:

$$\mathbf{P} = \begin{bmatrix} \sqrt{1-\phi^2} & 0 & \cdots & 0 & 0 \\ -\phi & 1 & 0 & \vdots & 0 \\ 0 & -\phi & 1 & \ddots & \vdots \\ \vdots & \ddots & \ddots & \ddots & \vdots \\ 0 & \cdots & 0 & -\phi & 1 \end{bmatrix} \tag{7}$$

For the case of the first element in the matrix, the AR(1)-model can not be constructed. Thus, the influence of the autocorrelation is approximated by $\sqrt{1-\phi^2}$. If the time series has a gap between index t and $t-1$ (i.e. $X_t - X_{t-1} > 1$), the autocorrelation ϕ in Eq. (7) is set to 0 for this element.

Finally, the matrix $\mathbf{P}$ is then used to transform the fit function of Eq. (2) into the autocorrelation space:

$$\mathbf{P}Y_t = Y_t' = \mathbf{P}(\mathbf{M_t}x + N_t) = \mathbf{M_t'}x + \varepsilon_t \tag{8}$$

The system of linear equations in Eq. (8) can then be solved by simple linear algebra in which the fit errors of the estimators already include the contribution from the autocorrelation of the noise.

One limitation of the AR-model is the assumption of stationarity of the variance. Although this limitation can be overcome by using ARMA (auto-regressive moving average) or ARIMA (auto-regressive moving integrated moving average) processes, the determination and application of these models (for example in the transformation of the linear equation system of the fit function) is highly non-trivial, especially for the case of unevenly spaced time series. Although an ARMA(1,1) process would be possible in the case that the lag-1 and lag-2 coefficients of the autocorrelation function have the same sign (e.g. Foster and Rahmstorf, 2011), this condition is not always given in our case. Thus, we have decided to stay with the AR(1) process.

3 Trend results

At this point, we would like to note that, especially in the high latitudes, complete temporal coverage within the MPIC OMI TCWV data set is not always given. For example, the winter months are often missing because no satellite measurements are available due to the seasonal solar cycle or ice cover. Thus, the trends shown are not representative for the entire year, but only for part of it, and should be interpreted with caution. However, we would still like to present the results, as these regions are of great interest in climate research. A map depicting the fractional temporal coverage is provided in Fig. S1 in the Supplement.

Moreover, when investigating climatological trends of TCWV on local scale, these are also influenced by changes in atmospheric dynamics and should therefore be judged with caution. Nevertheless, they can still provide us information about changes of the large-scale TCWV distribution.

3.1 OMI TCWV trends

To obtain reliable results, the trend analysis is performed only for grid cells whose time series cover at least half of the complete time period of interest. The results of the trend analysis of the OMI TCWV data set for the time range from January 2005 until December 2020 are illustrated in Figure 2.

The top row shows the absolute trends b (Fig. 2a) and the relative trends $\frac{b}{m}$ (Fig. 2b), respectively. Overall, increasing TCWV amounts are obtained: the absolute trends show high values in the equatorial Pacific and Southeast Asia and the relative trends reveal high values in North America, the North Pacific, and Southeast Asia. However, also negative values in the TCWV trends can be observed, e.g. in the region of the South Pacific convergence zone, South Africa, Brasil, and the equatorial Atlantic. Altogether, we obtain a global area-weighted (i.e. weighted by the cosine of the latitude) mean absolute TCWV trend of $+0.056\,\mathrm{kg\,m^{-2}\,y^{-1}}$ $+0.054\,\mathrm{kg\,m^{-2}\,y^{-1}}$ and a relative TCWV trend of approximately $+0.24\,\%\,\mathrm{y^{-1}}$$+0.21\,\%\,\mathrm{y^{-1}}$. We also obtained distinctively high trend values over mountains such as the Himalayas and Andes. However, these high values are likely artefacts due to uncertainties of the satellite retrieval, for example in the input data for the ground elevation. Thus, we decided to filter these artefacts and only show grid cells for which the mean ground elevation is lower than 3000 m above mean sea level based on the GMTED2010 elevation data set (Danielson and Gesch, 2011).

The linear least-squares fit assumes that errors of the estimators are normal distributed. Thus, we can perform a Z-test from the fit results and determine which trends are statistically significant or not. For our purpose we choose a significance level of 5%, for which the Z-test requires that $|b| \geq 1.96\sigma_b$ (see Fig. 2c and 2d). Furthermore, to account for test multiplicity and field significance, we additionally perform a false discovery rate (FDR) test (Benjamini and Hochberg, 1995; Wilks, 2006, 2016). Because the OMI TCWV data set also shows a high spatial autocorrelation (see Appendix B), we follow the recommendations in Wilks (2016) and choose a significance level of 2.5% for the FDR test.

The remaining trends are given in the bottom row of Fig. 2 with absolute and relative trends in Panels (ce) and (df), respectively. From the about 13000 12500 trends originally classified as significant according to the Z-test, approximately 4000 4700 grid cells still remain significant after the application of the FDR test and almost all of them reveal a positive TCWV trend, in particular

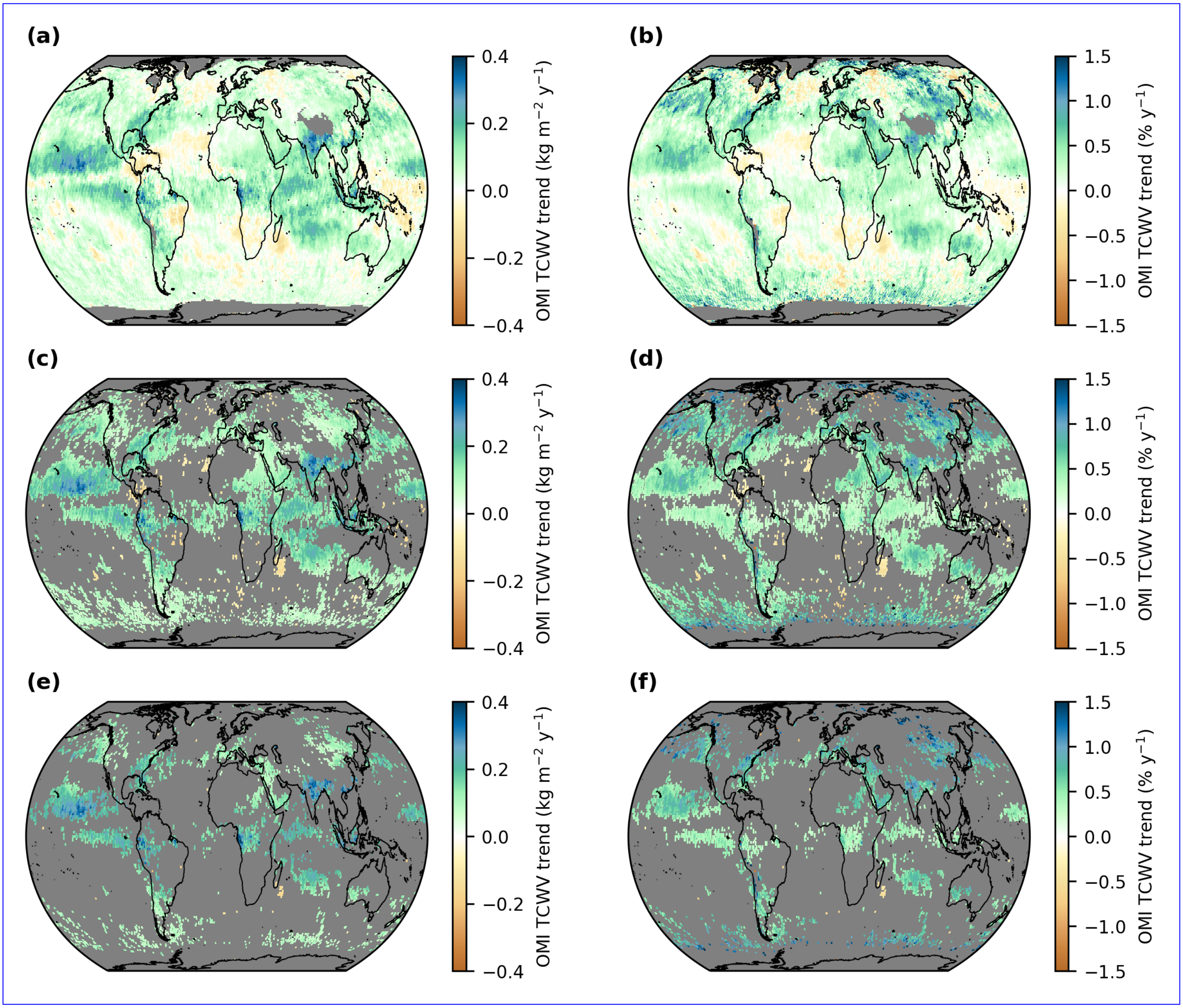

Figure 2. Global distributions of TCWV trends (2005-2020) derived from the MPIC OMI TCWV data set. Panels (a) and (b) depict the calculated absolute and relative TCWV trends, respectively. The bottom row depicts all remaining significant trends (absolute Panels (c) and relative (d) depict significant absolute and relative trends, respectively, after the application of the Z-test. Panels (e) and (f) depict significant absolute and relative trends, respectively, after the application of the Z-test and the FDR test. Grid cells for which no trend could be calculated (Panels (a) and (b)) and/or for which the trends do not fulfill the significance criteria (Panels (c) and (d)c-f) are coloured grey.

over the Pacific ocean, East Asia, and parts of the US East coast.

In addition to the TCWV trends, we also analyze the trends of the individual components of the DOAS retrieval, i.e. the slant column density (SCD) and the airmass factor (AMF), where TCWV=SCD/AMF. These additional analyses reveal that the TCWV trends are mainly determined by trends in the SCD, i.e. by increasing or decreasing H_2O absorption due to respectively changing atmospheric water vapour content. The trends of the inverse AMF (i.e. 1/AMF) are generally negative, but also distinctively weaker (about 3-4 times) than the SCD trends and thus have only a moderate influence on the overall TCWV trends. More details on these analyses are given in Appendix C.

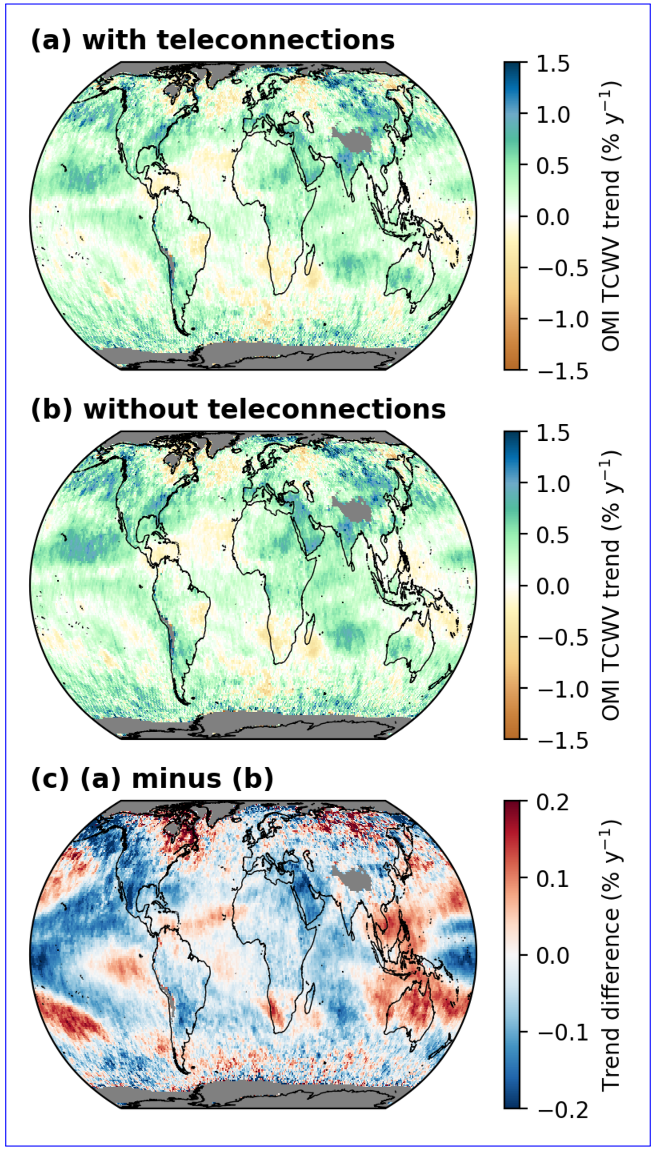

Figure 3. Global distributions of TCWV trends (2005-2020) derived from the MPIC OMI TCWV data set. Panels (a) and (b) depict the calculated relative TCWV trends with and without teleconnections indices, respectively, in the trend analyses. Panel (c) depicts the trend difference with minus without teleconnections. Grid cells for which no trend could be calculated are coloured grey.

To highlight the influence of teleconnections on the trend results for the OMI TCWV data set, we also perform the trend analysis not accounting for them. The resulting trends and their difference are shown in Figure 3. While overall the spatial distributions of the relative trends (Fig. 3a & b) look quite similar, distinct patterns emerge when looking at the trend difference (Fig. 3c): for instance the typical PMM and ENSO teleconnection patterns are clearly visible (e.g. dipole structure over the maritime continent in the case of ENSO). Consequently, the resulting deviations are particularly strong in the tropical and subtropical Pacific and can reach values as high as the relative trends themselves.

We have also tested other AR-models with lag=2, 3, 6, and 12 and found that the trend results as well as the distributions of the significant trends differ only slightly from those using an AR(1) model. The corresponding trend results can be found in Fig. S2 in the supplement.

3.2 Intercomparison to trends of other TCWV data sets

To verify the OMI TCWV trends and to detect potential shortcomings within the OMI TCWV data set, we performed the analyses also for monthly mean TCWV data from the reanalysis model ERA5 (Hersbach et al., 2019, 2020). For this purpose, the ERA5 TCWV data set is gridded on a $1° \times 1°$ lattice. Moreover, to account for OMI's observation time (13:30 LT), we only take into account ERA5 monthly mean values between 13:00-14:00 LT.

The resulting trend maps maps of the relative trends are given in Figure 4. Overall, the trend results of OMI and ERA5 agree well to each other: both absolute and all and only significant relative trend results (top and bottom row in Fig. 4, respectively) have similar strengths and also show similar global distributions. Nevertheless, the OMI TCWV trends reveal slightly stronger increases over parts of East Asia (which are also classified as significant) and South America and are in general less smooth than the ERA5 results. Similar findings can be obtained for the absolute trends, which are available in Fig. S3 in the Supplement.

In addition to ERA5, we also compare the trend results to trends from the TCWV satellite product GOME-Evolution (Beirle et al., 2018). Since the GOME-Evolution product is only available until 2015, we modified the time range accordingly, i.e. the results for the relative trends shown in Fig. 5 (and for the absolute trends in Fig. S4) correspond to a time range from January 2005 to December 2015. The distributions of both trend results share many similar patterns with While the distributions of the relative trends have quiet similar patterns and partly similar magnitudes, apart from some regionsfor instance in North Americastriking differences can be seen in some regions: For example, the OMI trends in the tropical Pacific North America or the Arabian Peninsula are much higher than the GOME-Evolution trends. Also, overall, many more trends are classified as significant for OMI than for GOME-Evolution. Considering

Nevertheless, considering that the GOME-Evolution product retrieves total column water vapour in the „visible red" spectral range, uses a different vertical column density (VCD) conversion scheme (see also Wagner et al., 2003, 2007; Grossi et al., 2015) and observes the atmosphere at an earlier overpass time (around 10:00 LT), the good agreement in the trend results further confirms the reliability of the findings of the OMI TCWV trend analysis.

Furthermore, we made additional comparisons to the results of past studies. From these comparisons, several differences in the strength and spatial distribution of TCWV trends emerge. The reasons for these differences are on the one hand the

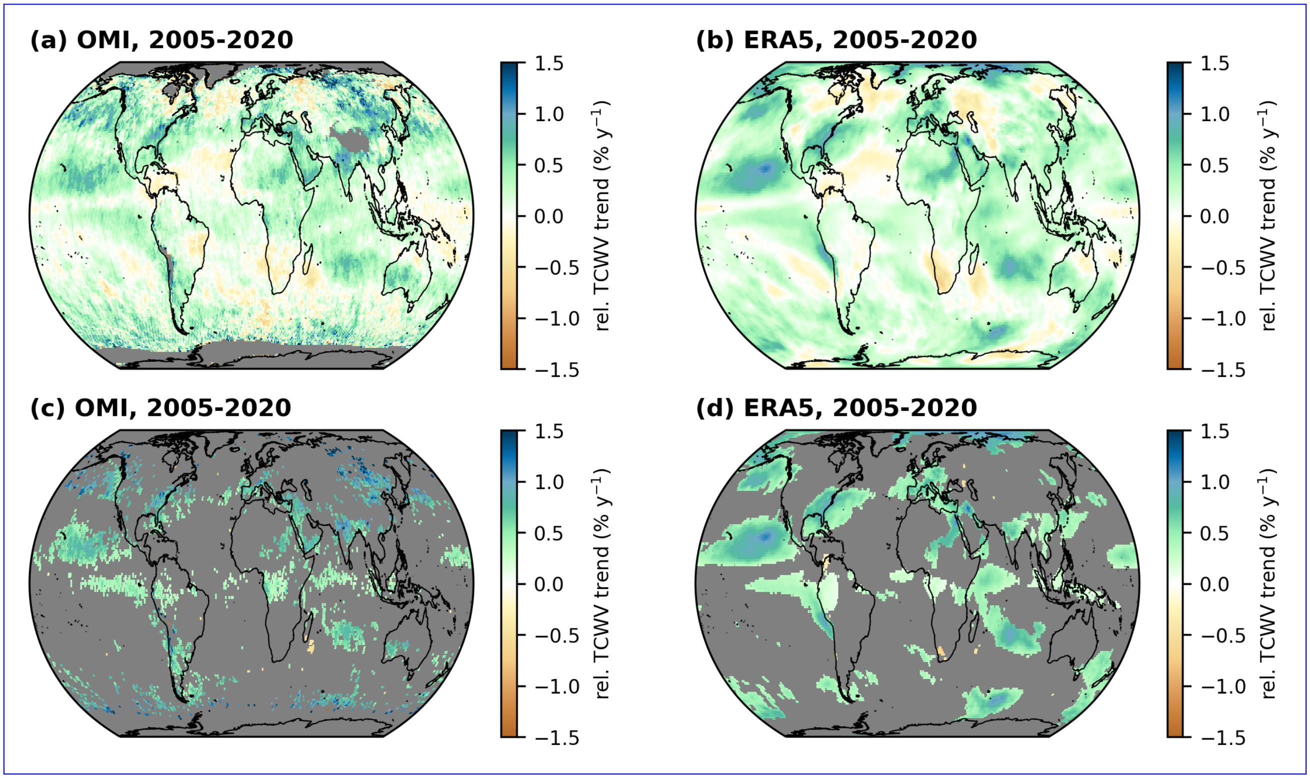

Figure 4. Global distributions of relative TCWV trends derived from the OMI TCWV data set (left column) and ERA5 (right column). Panels (a) and (b) depict the all calculated absolute relative TCWV trends and panels (c) and (d) the corresponding relative TCWV significant trends remaining after the application of the Z-test and FDR test. Grid cells for which no valid trend could be calculated are coloured grey.

consideration of different time periods, and on the other hand also different methods of analysis. Further details about these comparisons can be found in the Appendix D.

4 Trends in relative humidity

In this section, we investigate to what extent the assumption of constant relative humidity is given at local scale. For this purpose, we make the following assumptions: First, we assume that the relative changes in TCWV correspond to those in near-surface specific humidity q_s, i.e. $\frac{d\mathrm{TCWV}}{\mathrm{TCWV}} \approx \frac{dq_s}{q_s}$. This assumption should be fulfilled since TCWV is directly connected to the specific humidity via its vertical integral and approximately 60% of the TCWV is located within in the planetary boundary layer. Second, we also assume that relative changes of specific humidity correspond to changes in water vapour pressure, i.e. $\frac{dq}{q} \approx \frac{de}{e}$ (assuming that relative changes in surface air pressure are negligible, i.e. $\frac{dp_s}{p_s} \ll \frac{de}{e}$). Given the aforementioned assumptions and that the water vapour pressure e can be described as $e = \mathrm{RH} \cdot E$, we can derive the relative changes in relative humidity (RH) by combining the relative TCWV trends with trends in surface air temperature T:

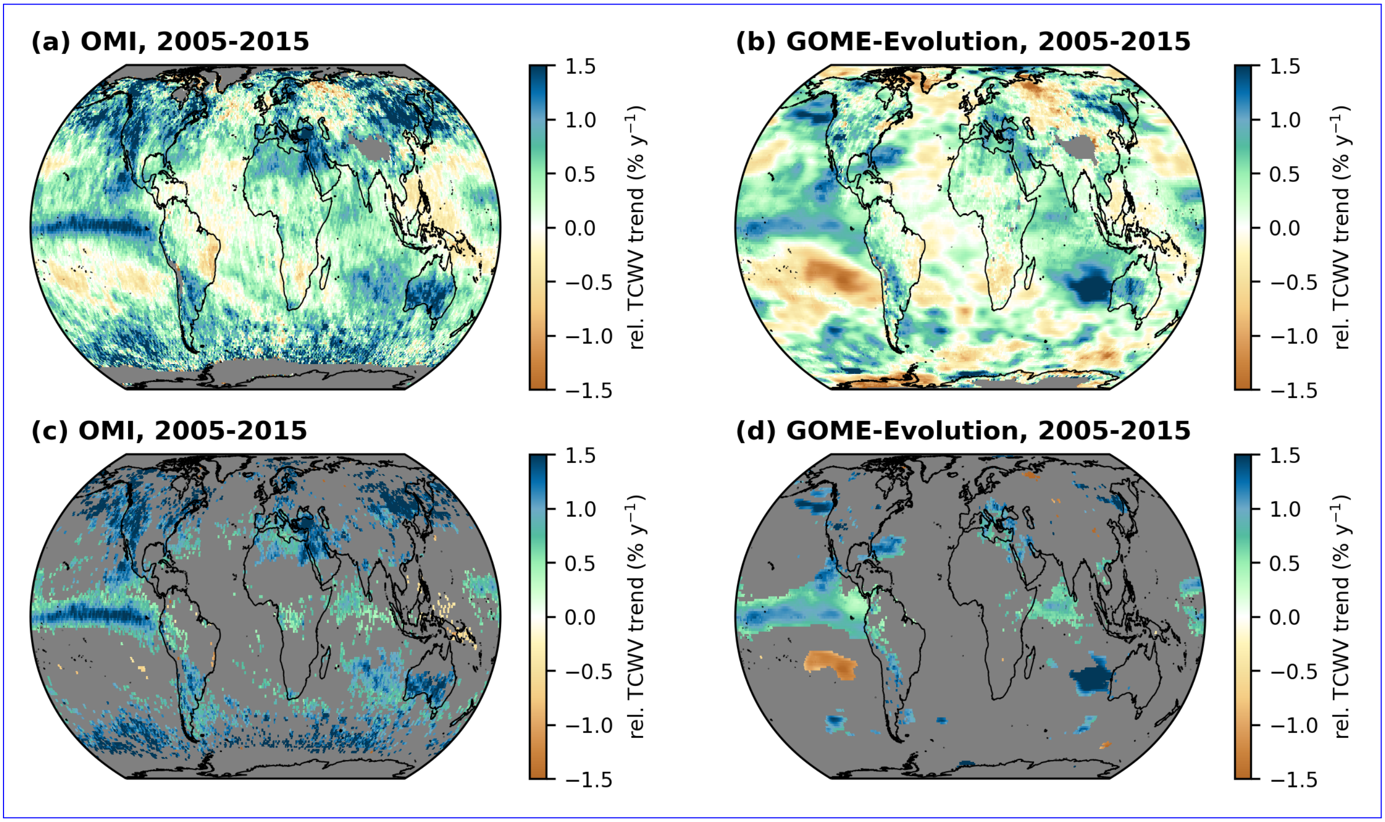

Figure 5. Global distributions of relative TCWV trends derived from the OMI TCWV data set (left column) and GOME-Evolution (right column) for the time range from January 2005 to December 2015. Panels (a) and (b) row depict the all calculated absolute relative TCWV trends and Panels panels (c) and (d) the corresponding relative TCWV significant trends remaining after the application of the Z-test and FDR test. Grid cells for which no valid trend could be calculated are coloured grey.

$$\frac{dq_s}{q_s} \approx \frac{de}{e} = \frac{d\mathrm{RH}}{\mathrm{RH}} + \frac{dE}{E} \tag{9}$$

$$\rightarrow \frac{d\mathrm{RH}}{\mathrm{RH}} = \frac{dq_s}{q_s} - \frac{L_v(T)}{R_v}\frac{dT}{T^2} \approx \frac{d\mathrm{TCWV}}{\mathrm{TCWV}} - \frac{L_v(T)}{R_v}\frac{dT}{T^2} \tag{10}$$

Thus, if RH is 50%, a relative increase of 1% indicates an absolute RH increase of 0.5 %. However, it should be noted that the largest uncertainties lie in the first assumption, i.e. slight under- or overestimations of the actual relative q_s-changes will cause corresponding deviations in the relative RH changes.

Figure 6 depicts the resulting relative RH trends derived from the OMI TCWV trends in combination with the temperature trends from the Berkeley Earth temperature data record (Rohde and Hausfather, 2020) and from ERA5 as well as the relative RH trends from the HadISDH surface relative humidity data set (Willett et al., 2014, 2020). In general, the results for OMI and ERA5 reveal a global (relative) increase in RH, especially the trends over ocean are widely positive. However, in all three data

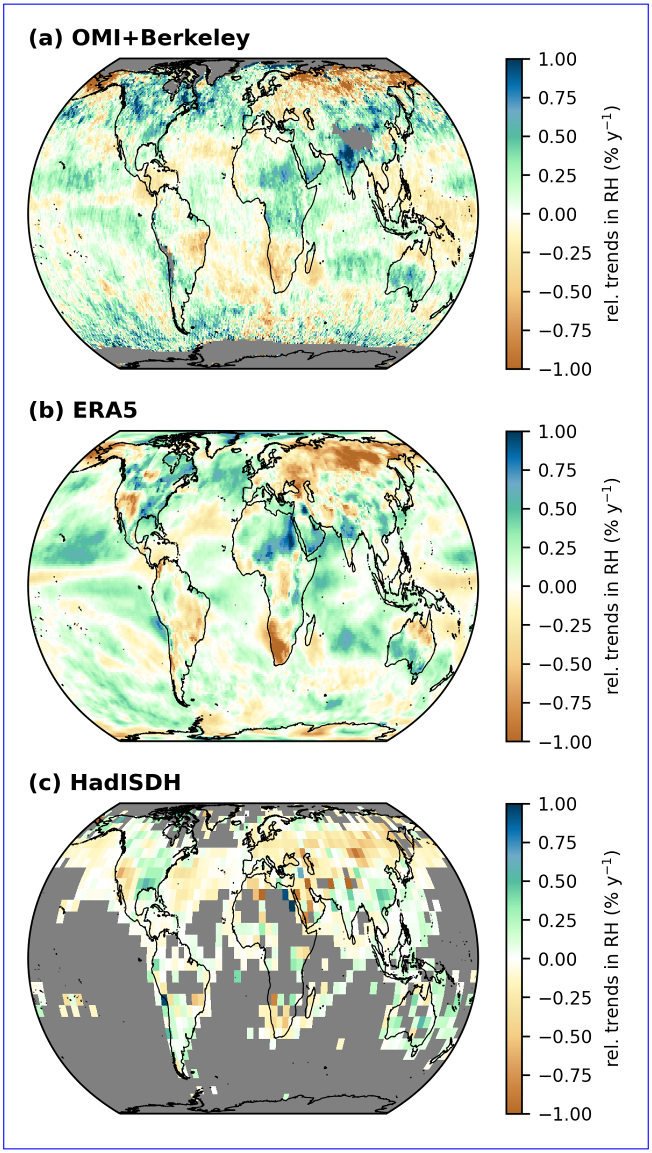

Figure 6. Relative trends in relative humidity (RH) derived from the relative TCWV trends and the temperature trends from OMI and Berkeley Earth (a) and from ERA5 (b) and from the data set HadISDH (c) for the time range January 2005 to December 2020. Grid cells for which no trend has been calculated are coloured grey.

sets distinctive decreasing trends are observable over land, for instance over Russia or South Africa. Considering the differences in the selected time period and measurement source, the RH trends from OMI over land surface coincide well with the results from Dunn et al. (2017). Interestingly, The reduction in relative RH over land is likely related to marked land-ocean contrast in warming, (besides various local factors such as changes in vegetation cover) (Simmons et al., 2010; Fasullo, 2012): Over ocean, due to the direct link with sea surface temperature, the water vapour content can increase adequately to keep RH constant. Over land, this is usually only possible with a delay due to limited water availability, as water must first be transported there from the ocean. Since the temperature also increases much more over land than over the ocean, the decrease in RH might be due to the lack of an increased water supply from the ocean (Simmons et al., 2010).

Interestingly, we also find distinctive increases of RH can be found in arid regions (e.g. over the Sahara) as well as distinctive decreases in humid regions (e.g. the tropical Pacific ocean) within the OMI as well as the ERA5 results. Recently, Bourdin et al. (2021) investigated RH trends from the reanalysis models ERA5 and JRA-55 over the past 40 years and also found significant negative trends in the tropical lower troposphere.

Several studies have shown that global warming will lead to a further drying of dry regions (e.g. Sherwood and Fu, 2014) and wet regions will become even wetter (e.g. Held and Soden, 2006; Chou et al., 2013; Allan et al., 2010), leading to the simple paradigm of "dry gets drier, wet gets wetter" (DDWW) (Chou et al., 2009). In addition, other studies show that changes in precipitation correlate very well with changes in ocean salinity, suggesting a "fresh gets fresher, salty gets saltier" pattern (Cheng et al., 2020, and references therein). Though most of these studies focus on changes in precipitation, our results for RH support the findings from Greve et al. (2014) and Byrne and O'Gorman (2018) that the DDWW-paradigm is not always fulfilled over land. Surprisingly, according to our results, this paradigm is not fulfilled even over the tropical Pacific ocean, the region on which most of the concepts of the studies are based (e.g. Held and Soden, 2006). However, we would like to stress here that the time period studied is probably too short to question the paradigm.

5 Relationship between TCWV and precipitation

According to Bretherton et al. (2004) and Rushley et al. (2018) a nonlinear relationship between TCWV (or column relative humidity, respectively) and precipitation exists for the tropical ocean. Thus, given the TCWV and RH trend results, we expect to observe a decline or negative trend in particular over the Pacific ocean along the intertropical convergence zone. For the analysis of trends in precipitation we use the monthly mean rain rates from the GPCP Version 3.1 3.2 Satellite-Gauge (SG) Combined Precipitation Data Set (Huffman et al., 2020). For the sake of consistency we grid the GPCP data from a resolution of $0.5° \times 0.5°$ to a $1° \times 1°$ lattice. Note that at the time of the preparation of this manuscript, the GPCP data was only available until December 2019.

Although precipitation climate data records (CDRs) allow a global analysis, they are subject to large uncertainties, as satellite and rain-gauge observations do not have good spatio-temporal coverage, weak and short rain events are not well detected or even missed, and satellite retrievals can determine the rain rate only indirectly. Thus, deviations of about 50% in the daily rain rate can occur compared to in situ measurements (e.g. Prat et al., 2021). Nevertheless, Prat et al.

(2021) show that over accumulation periods of month or years, precipitation CDRs perform satisfactorily. Moreover, Prat et al. (2021) used an older GPCP version (v2) than ours in their evaluation study.

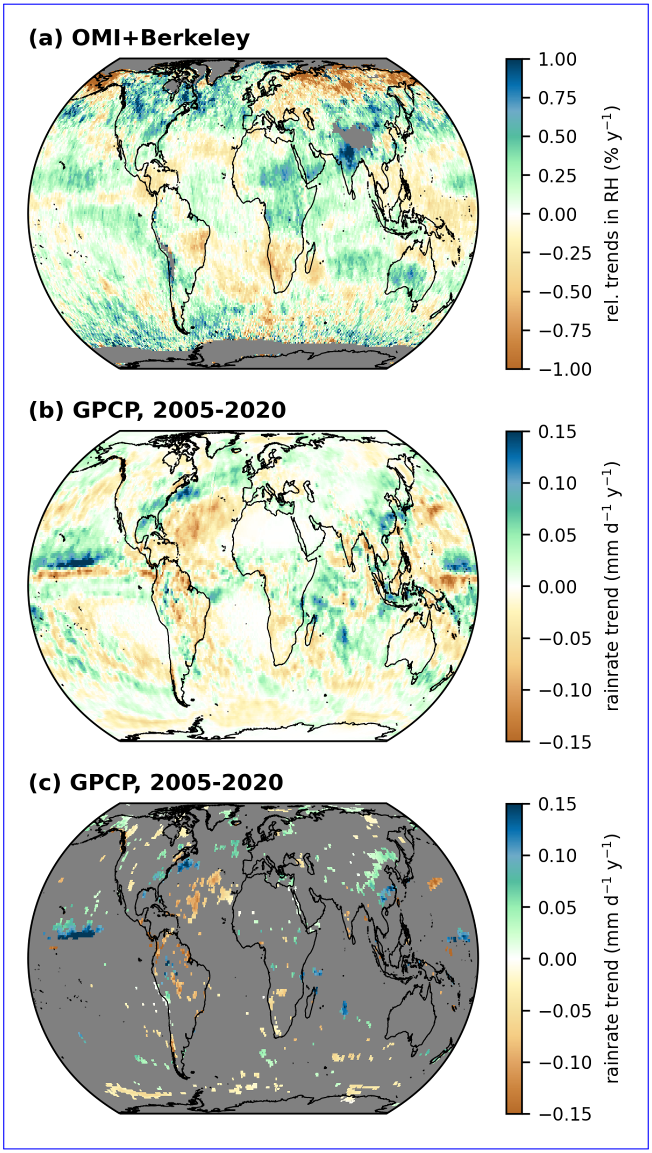

Figure 7. Global distribution of relative RH trends derived from OMI TCWV data set (time range 2005 to 2020) (Panel (a), same as in Fig. 6a) and of trends in precipitation derived from GPCP v3.1 .2 monthly mean data set for the time range from January 2005 to December 2019 (2020. Panel (b) depicts all rain rate trends and Panel (c) only those that are considered significant after applying the Z-test (to the significance level of 5%) and a FDR test (see also Appendix B). Grid cells for which no trend has valid trends have been calculated are coloured grey.

Figure 7 depicts the obtained trends in precipitation as well as the relative RH trends from OMI. Comparing the trend distributions of the monthly mean rain rates to the relative RH trends, negative and positive trends in precipitation and RH match quite well in the tropics and subtropicsover the tropical and subtropical ocean, especially over the tropical Pacific ocean. Hence, the discrepancies between our observations and the expected changes in the hydrological cycle make evident that accurate observations and long-term monitoring of the Earth's hydrological cycle and atmosphere on global scale from multiple remote sensing and in situ platforms are essential to clarify this important aspect.

6 Global responses of the hydrological cycle to global warming

5.1 Sensitivity of TCWV to changes in surface air temperature

Under the assumption of invariant relative humidity, the CC-equation yields that a temperature change of 1 K leads to a change in water vapour by about 6-7% (Held and Soden, 2000) for the case of typical atmospheric conditions.As we have demonstrated in Sect. 4, this assumption is not always fulfilled neither over land nor over ocean on local scale. Thus, we check how strong the deviations from the CC-response are on global scale. To reduce the influence of potential changes on the local scale and the Northern subtropical Atlantic. While over land within the subtropics an acceptable match can be determined in some regions (e.g. South Africa, Brazil), the patterns of the relative RH and rain rate trends no longer match well towards mid and high latitudes (e.g. changes in local circulation patterns), we calculate the global, zonal averages of the OMI and ERA5 TCWV data sets for each time step and then derive the trends from each of the respective averages. After that, we combine the global OMI TCWV trends with either the global temperature trends from the Berkeley Earth temperature data record (Rohde and Hausfather, 2020) (OMI+Berkeley) , or the temperature trends from HadCRUT5 data set (Morice et al., 2021) (OMI+HadCRUT5) , and the ERA5 TCWV trends with the respective ERA5 temperature trends (both representative for 13:00-14:00 LT, see in North America), likely because in these regions the rain rate is mainly determined by atmospheric dynamics (cyclone or storm tracks) rather than thermodynamics. Furthermore, the distinctive increases of relative RH in the mountainous regions of South America (Andes) and northern India (Himalayas) are likely due to the inadequacies in the OMI TCWV satellite data caused by the complex topography (see also Sect. 3.2)and evaluate the changes in TCWV for changes in air temperature . For the case of the temperature data record of HadCRUT5, we regridded the OMI TCWV data set to the spatial resolution of HadCRUT5 (i.e. $5^\circ \times 5^\circ$) and performed the trend analysis accordingly.

Meridional mean rate of change of TCWV (% K^{-1}) for OMI in combination with the temperature from Berkeley Earth and HadCRUT5 and for ERA5 (solid lines). The dashed lines represent the theoretically expected CC-response based on the mean air temperature of the respective temperature data sets from the trend analysis.

Figure **??** illustrates the corresponding results as a function of latitude between 60°S and 60°N.Theoretically, if relative humidity remained constant, the TCWV response should vary around values close to the coloured dashed lines representing the CC-response. However, the rate of change shows strong fluctuations and varies mostly around 10 % K^{-1} within the lower latitudes, and increases towards higher latitudes to values 2 or 3 times higher than the CC-response. In contrast to O'Gorman and Muller (2010) we do not find a local maximum in the southern high latitudes but rather in the northern high latitudes at around 55°N. Interestingly, a local maximal rate of change for ERA5 is located in the northern subtropics between 15-20°N3.1).

Given that the TCWV response even on global scale is mostly stronger than the expected CC-response, the results for the rate of change further confirm that relative humidity does not remain invariant even Trenberth (2011) and Trenberth and Shea (2005) analysed local correlations between precipitation and surface temperature for cold and warm seasons and reported mainly positive correlations over ocean and negative correlations year round over land throughout the tropics. However, over ocean the correlations also depend on whether the (sea) surface temperature is driven by the ocean or by the atmosphere (Trenberth and Shea, 2005). While in some regions of the subtropics we can also find this high correlation in the trend patterns of precipitation and surface temperature (e.g. increase in precipitation in the northern subtropics in the eastern Pacific or decrease in the subtropical Atlantic over ocean; decrease in Brazil or South Africa over land), we cannot find a direct link for the striking negative precipitation trends in the equatorial Pacific. However, it should also be taken into account that a large part of the precipitation trends are not statistically significant.

Overall, the discrepancies between our observations and the expected changes in the hydrological cycle make evident that accurate observations and long-term monitoring of the Earth's hydrological cycle and atmosphere on global scale but instead seems to increase with time (at least for the time range of our investigations). This contradicts the findings from Dai (2006) who found a non-significant trend in relative humidity of around +0.6 % decade^{-1} from 1974-2004 and the findings from Dunn et al. (2017) who derived a negative trend for global-averaged *land* surface relative humidity for the time period 1996-2015from multiple remote sensing and in situ platforms are essential to clarify this important aspect.

5.1 Changes in the atmospheric water vapour residence time

6 Changes in the atmospheric water vapour residence time

Another key diagnostic of the hydrological cycle is the atmospheric water vapour residence time (WVRT). The WVRT can help to better understand changes in dynamic and thermodynamic processes within a changing climate (Trenberth, 1998; Gimeno et al., 2021): for instance an increase in WVRT suggests that the length of the atmospheric moisture transport increases, i.e. the distance between moisture sink and source regions (Singh et al., 2016). Several different metrics exist for quantifying the WVRT (van der Ent and Tuinenburg, 2017; Gimeno et al., 2021), howeverbearing in mind that the WVRT distribution or the lifetime distribution (LTD) is exponential on local scale and thus the mean value is strongly influenced by a few high values (van der Ent and Tuinenburg, 2017; Sodemann, 2020). Ideally, one would determine the LTD for each grid cell for each month from backward trajectories and then examine their changes or trends. However, this would be well beyond the scope of this paper.

Thus, for our purpose and for the sake of simplicity we focus on the so called depletion time constant (DTC) and the turnover time (TUT). The TUT describes the global average mean age of precipitation and can be calculated as the ratio of TCWV to precipitation P:

$$\mathrm{TUT} = \frac{\overline{\mathrm{TCWV}}}{\overline{\mathrm{P}}} \tag{11}$$

where the bar indicates global average. Typically, the TUT varies between values of 8 to 10 days and is expected to increase by 3–6 % K^{-1} (Gimeno et al., 2021, and references therein). Basically, it is also possible to calculate the TCWV/P ratio on local scale and determine a depletion time constant (e.g. Trenberth, 1998). However, it must be taken into account that the WVRT distribution or the lifetime distribution (LTD) is exponential on local scale, so that the mean value is strongly influenced by afew high values (van der Ent and Tuinenburg, 2017; Sodemann, 2020). Thus, one ideally would determine the LTD for each grid cell for each month from backward trajectories and then examine their changes or trends. However, this would be well beyond the scope of this paperAnalogously, the DTC is defined as the local ratio of TCWV to precipitation (e.g. Trenberth, 1998):

$$\mathrm{DTC} = \frac{\mathrm{TCWV}}{\mathrm{P}} \tag{12}$$

The DTC values might vary substantially from TUT, but the global precipitation weighted average is equal to TUT (Gimeno et al., 2021).

For our investigations of trends in DTC we combine the regridded GPCP data set from Sect. 4 and the OMI TCWV data set and perform the trend analysis scheme from Sect. 2.2 to the monthly DTC values for the time range 2005 to 2020. To ensure numerical stability, we only consider monthly rain rates greater than $0.25\,\mathrm{mm\,d^{-1}}$. As a result, large parts of the subtropical oceans and deserts are excluded from the analysis.

The results of the DTC trend analyses are depicted in Figure 8. On average, we typically obtain mean DTC values between 5-10 days in the areas where rain occurs (Fig. 8a). In the subtropical dry zones, values of around 30 days and well above are found. In terms of absolute DTC trends, the most striking patterns are in the northern subtropical Atlantic with strong increases and in the northern subtropical western Pacific with strong decreases. In comparison, the distribution of relative DTC trends is much spottier, but overall, in addition to the patterns already mentioned, we obtain distinctive increases in DTC on the US west coast, in Europe, Russia and in the eastern Pacific.

For our investigations of trends in TUT we first calculate global averages of the regridded GPCP data set from Sect. 4 and the OMI and ERA5 TCWV data sets between 60°S and 60°N for each month, then combine the time series of global averages, and finally perform the trend analysis for the TUT time series for the time range from 2005 to 2019. 2020.

The results of the respective trend analyses are summarized in Table **??**. Typically, changes in TUT on global scale are mainly dominated by changes in TCWV, as TCWV is much more sensitive to changes in temperature than precipitation. Interestingly, for our case, the increase in TUT is due to a combination of Altogether, we find an increase in TCWV and a decrease in precipitation. Altogether, the results the global TUT for OMI and ERA5 are almost identical with an increase in the TUT by approximately $+0.02\,\mathrm{d\,y^{-1}}$ or $+0.23\,\%\,\mathrm{y^{-1}}$of approximately $+0.02\,\mathrm{d\,y^{-1}}$ with TUT mean values of around 9.7 d for OMI and 8.8 d for ERA5. Combining the long-term relative trends in TUT and trends in surface air temperature, we estimate a TUT rate of change of about $11.58\,\%\,\mathrm{K^{-1}}$ for can estimate the sensitivity of TUT to global warming r, i.e. $r = \frac{\Delta \mathrm{TUT}}{\mathrm{TUT}}/\Delta \mathrm{T}$. For the case of OMI and Berkeley Earthand $10.78\,\%\,\mathrm{K^{-1}}$, we find a TUT sensitivity of around $8.4\,\%\,\mathrm{K^{-1}}$ and for ERA5 which is approximately 2 to 4 times of around $8.8\,\%\,\mathrm{K^{-1}}$ which is higher than the results of $3–6\,\%\,\mathrm{K^{-1}}$ pooled in Gimeno et al. (2021).

7 Summary

In this study, we analyzed global trends within a long-term data set of total column water vapour (TCWV) retrieved from multiple years of OMI observations for the time period January 2005 until December 2020 and considered the effects of autocorrelation of the residuals within the analysis scheme. The results of the analyses were then put into context to trends from additional TCWV data sets like from the GOME-Evolution project or from the reanalysis model ERA5 and overall very good agreement was found. In a next step, based on the relative OMI TCWV trends, trends in relative humidity were derived

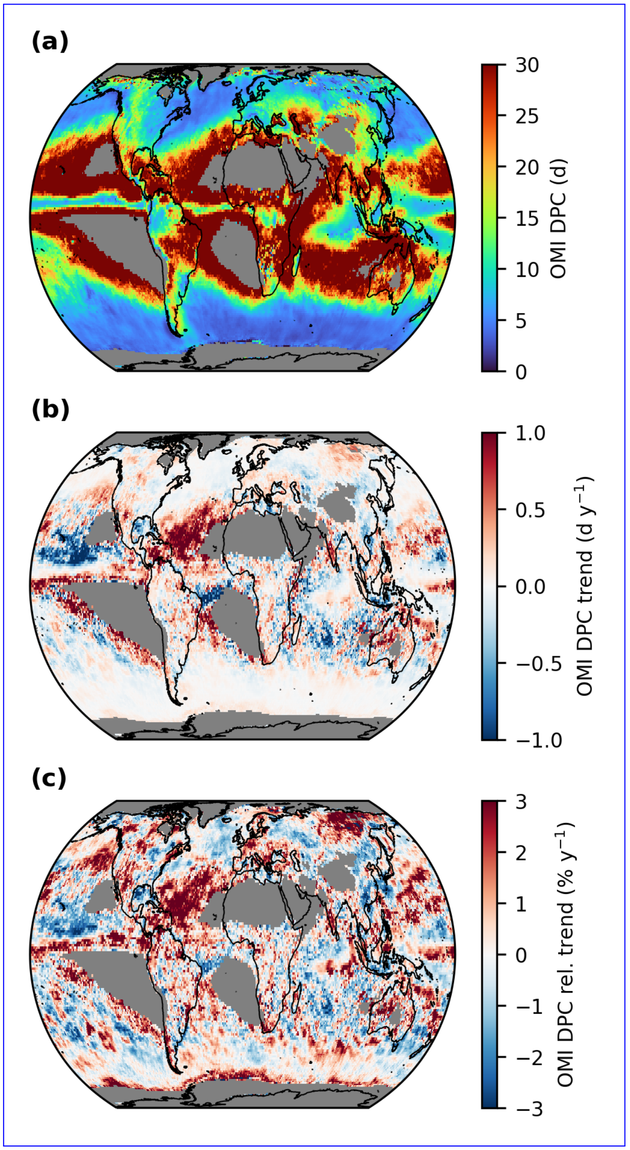

Figure 8. Summary Global distribution of annual DTC trends (absolute and relative) of the different parameters and data sets of the atmospheric hydrological cycle for the time range January 2005 to December 2019.2020. Panel (a) depicts the distribution of the mean DTC. Panels (b) and (c) depict the absolute and relative DTC trends. Grid cells for which no valid trend has been calculated are coloured grey.

Parameter Data set Absolute trend Relative trend OMI +0.060 kg m^{-2} +0.202 % ERA5 +0.055 kg m^{-2} +0.205 % Precipitation GPCP V3.1 −8 × 10^{-4} mm d^{-1} −0.029 % Berkeley Earth +0.020 K ERA5 +0.022 K OMI +0.021 d +0.231 % ERA5 +0.022 d +0.234 %

and put into context of the assumption of invariant relative humidity. Also, the response of TCWV and Moreover, under consideration of the relationship between (column) relative humidity and precipitation, the patterns of the relative RH trends have been compared to rain rate trends. Also, the changes in the the water vapour turnover time residence time and its response to changes in surface air temperature were investigatedunder consideration of theoretically expected TCWV responses based on the Clausius-Clapeyron (CC) equation.

The trend analysis reveals an increase in TCWV of approximately $+0.056\,\mathrm{kg\,m^{-2}\,y^{-1}}$ or $+0.24\,\%\,\mathrm{y^{-1}}$ $+0.054\,\mathrm{kg\,m^{-2}\,y^{-1}}$ or $+0.21\,\%\,\mathrm{y^{-1}}$ globally for the time period of January 2005 until the end of 2020. To determine if trends are significant or not, a Z-test as well as a false discovery rate test are applied to the trend results. After application of these significance criteria, almost all remaining trends are positive and distributed across the globe. However, particular spatial patterns remain, for instance within the region of subtropical northern East Pacific. Overall, the absolute and relative OMI TCWV trends agree well to the corresponding trends from ERA5 and from the GOME-Evolution data set.

To analyze if the assumption of temporally invariant relative humidity is fulfilled on local scale, we derived relative trends in relative humidity (RH) from the TCWV trends. All in all, we obtain that RH increases dinstinctively over large areas of the ocean and land surface. However, over both surface types also relative decreases can be well identified in some areas. Interestingly, relative decreases and increases in RH are not limited to arid and humid regions, respectively. For instance, our analysis reveals relative increases of RH over the (arid) Saharan desert and decreases of RH over the (humid) tropical Pacific ocean. Furthermore, within Within the tropics, we also find that the patterns of decreasing RH trends match those of decreasing precipitation quite well, especially within the tropical Pacific ocean.

Even after global averaging, the TCWV trends of OMI and ERA5 do not follow a CC-response: the TCWV response is approximately 2 to 3 times stronger than the theoretical CC-response, indicating that the assumption of invariant relative humidity is not fulfilled neither on local/regional nor on global scale. Furthermore, combining the trends of TCWV, Combining the TCWV and rain rate data sets, changes in the water vapour residence time (WVRT) have been investigated. Overall, an increase in the turnover time of about $+0.02\,\mathrm{d\,y^{-1}}$ has been observed. Together with the long-term trends surface temperature, and precipitation reveals that the global response of the water vapour turnover time (TUT) to changes in temperature is around $11\,\%\,\mathrm{K^{-1}}$ and thus we estimate a TUT sensitivity to global warming of around $8.4\,\%\,\mathrm{K^{-1}}$, which is 2 to 4 3 times higher than the values provided in Gimeno et al. (2021)with TUT trends of approximately $+0.02\,\mathrm{d\,y^{-1}}$.

All in all, our results show that several challenges still remain for a better understanding of the atmospheric hydrological cycle and even new questions arise regarding the complex interactions between air temperature, water vapour, precipitation and atmospheric dynamics. The differences between observed and expected changes in the hydrological cycle show that even on global scale simplified assumptions are not always valid (e.g. invariant relative humidity). Also, our observed, much higher global sensitivities of individual parameters of the hydrological cycle (i.e. TCWV and TUT) to changes in surface air temperature raise the question of what effects can be expected at the local scale (e.g. precipitation) with further increasing temperatures, especially with regard to changes in the global circulation such as the expansion of the Hadley cell towards higher latitudes (e.g. Staten et al., 2018; Borger et al., 2022)(e.g. Staten et al., 2018).

With regard to TCWV retrievals in the visible "blue" spectral range, there is great potential in extending the OMI TCWV data set with further satellite data (e.g. from TROPOMI or GOME-2) and combining it with future missions from geostationary satellites such as GEMS or Sentinel-4 which will also allow for investigations of (semi-) diurnal TCWV cycles.

Data availability. The MPIC OMI total column water vapour (TCWV) climate data record is available at https://doi.org/10.5281/zenodo.5776718 (Borger et al., 2021b)

.

Author contributions. CB performed all calculations for this work and prepared the manuscript together with SB and TW. TW supervised this study.

Competing interests. The authors have the following competing interests: Thomas Wagner is editor of ACP.

Acknowledgements. The ERA5 data (Hersbach et al., 2019) was downloaded from the Copernicus Climate Change Service (C3S) Climate Data Store. The results contain modified Copernicus Climate Change Service information 2021. Neither the European Commission nor ECMWF is responsible for any use that may be made of the Copernicus information or data it contains. The Dutch–Finnish-built OMI is part of the NASA EOS Aura satellite payload. KNMI and the Netherlands Space Agency (NSO) manage the OMI project. We acknowledge the NASA's Goddard Earth Sciences Data and Information Services Center (GES-DISC) for free access to the data.

Appendix A: Influence of ENSO and the autocorrelation on the trend results

To address the influence of ENSO and the autocorrelation on the trend results for the OMI TCWV data set, we perform the trend analysis not accounting for both of these effects.

Difference between absolute trends of the MPIC OMI TCWV data set (2005-2020) accounting minus not accounting for the influence of ENSO.

Figure ?? depicts the difference in the trend results accounting minus not accounting for the influence of El Niño within the trend analyses. The typical ENSO teleconnection patterns are clearly visible (e.g. dipole structure over the maritime continent). Moreover, the resulting deviations are particularly strong in the tropical and subtropical Pacific and can reach values as high as the trends themselves.

Difference between trends of the MPIC OMI TCWV data set (2005-2020) accounting minus not accounting for the influence of autocorrelation (Panel (a): absolute trends; (b): relative trends).

it. The panels in Fig. A1 illustrate the difference of the absolute (Panel (a)) and relative (Panel (b)) trends accounting minus not accounting for the effect of temporal autocorrelation. For high and mid latitudes the differences are close to zero indicating that the influence of the autocorrelation on the trend results is negligible. However, within the subtropics and tropics distinctive deviations are observable, especially in the regions where the autocorrelation is high (e.g. the Pacific ocean, see also Fig. 1). For the case of the relative trends (Fig. A1b) the deviations can reach up to $0.1\,\%\,y^{-1}$ $0.05\,\%\,y^{-1}$ (which is around 10% of the maximum magnitude of the relative trends in the affected regions) and consequently can cause wrong signs in the trend estimation (i.e. indicating a negative instead of a positive trend).

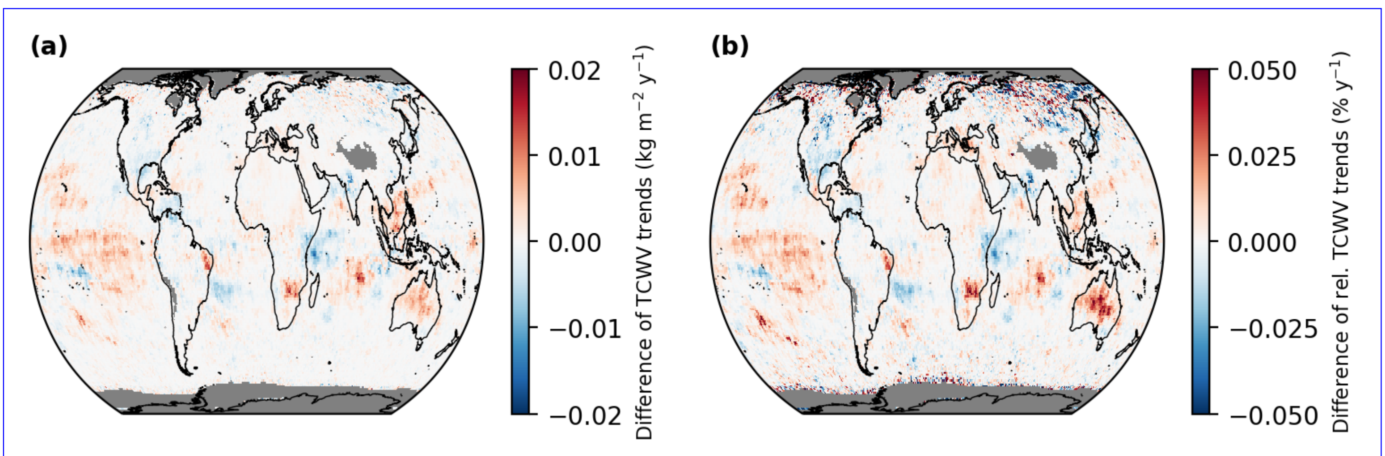

Figure A1. Difference between trends of the MPIC OMI TCWV data set (2005-2020) accounting minus not accounting for the influence of autocorrelation (Panel (a): absolute trends; (b): relative trends).

Appendix B: Spatial autocorrelation within the MPIC OMI TCWV and GPCP data set

The significance level at which the false discovery rate test method in Sect. 3.1 is performed depends on the degree of spatial autocorrelation. Thus, for every timestamp within the MPIC OMI TCWV data set, the spatial autocorrelation is calculated from the global TCWV distribution for gridpoint separations up to 7000 km.

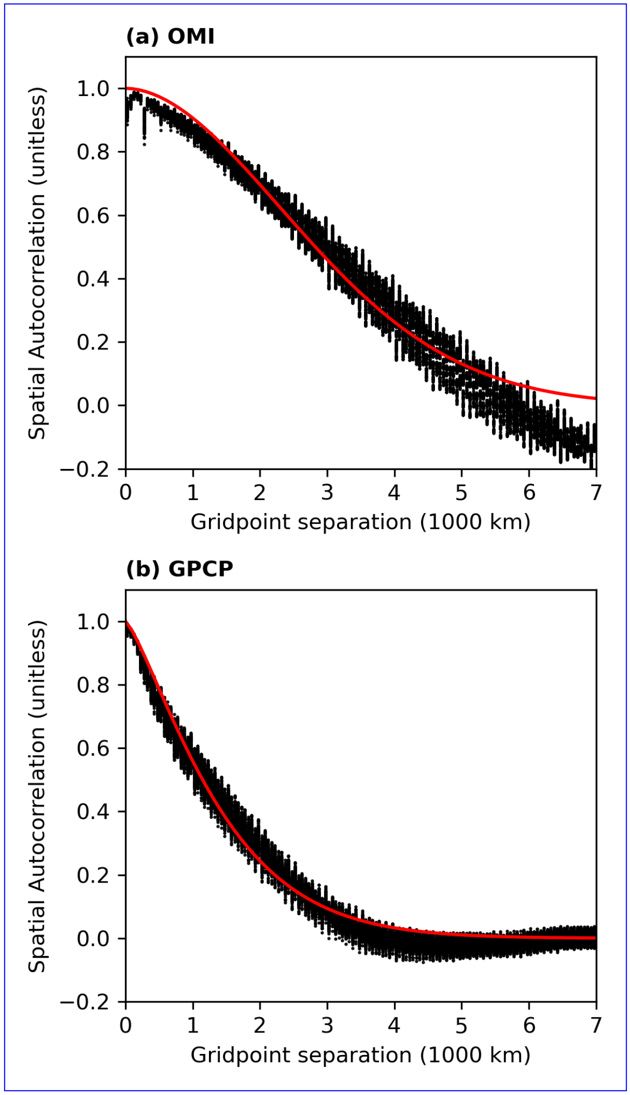

Figure B1. Spatial autocorrelation as function of the great circle distance of the MPIC OMI TCWV (Panel a) and the GPCP data set (Panel b). The black dots represent the results of the analysis of the TCWV spatial distribution for each time step in the TCWV respective data set. The solid red line illustrates lines illustrate the fit result of $f(x) = e^{-cd^2}$ $f(x) = e^{-a|x|^b}$.

Figure B1a illustrates the spatial autocorrelation of the OMI TCWV data set as a function of gridpoint separation. The red solid line is the fit result of $f(x) = e^{-cd^2}$ $f(x) = e^{-a|x|^b}$ with the gridpoint separation distance dx. For the OMI TCWV data set, we calculated a value of $c \approx 0.08$ $a \approx 0.098$ and $b \approx 1.88$, which equals an e-folding distance of approximately 3.55×10^3 km 3.43×10^3 km. According to Wilks (2016) this e-folding distance indicates a strong spatial dependency. Consequently, we follow the recommendations of Wilks (2016) and set for the FDR test the significance level to 2.5 % instead of 5.0 %.

The same procedure was applied to the GPCP dataset, the results of which are shown in Fig. B1b. For the fit results we get $a \approx 0.58$ and $b \approx 1.28$, which corresponds to an e-folding distance of 1.53×10^3 km and is thus less than half as large as that for TCWV. Accordingly, the spatial dependence is not so strong and the significance level for the FDR test can remain at 5% for the GPCP data set.

Appendix C: Trends of individual retrieval parameters

Here, we investigate to what extent the relative TCWV trends are due to geophysical changes in the water vapour content or due to changes in the retrieval input parameters. For DOAS retrievals, the TCWV amount as derived via the quotient of the integrated concentration along the light path (so called slant column density, SCD) and the so called airmass factor AMF, i.e. TCWV=SCD/AMF. Thus, the relative trends of these two quantities were calculated following the analysis scheme in Section 2.2. For the case of the SCD, we use the geometrical VCD (vertical column density), which is simply the SCD divided by the geometrical airmass factor (which remains constant over time).

The global distributions of the relative trends of both quantities are illustrated in Figure C1 (Panels (b) and (c)) as well as the relative TCWV trends (in Panel (a)). The distribution and strength of the geometrical VCD (Fig. C1b) largely coincide with the distribution of the relative TCWV trends (Fig. C1a). The trends of the inverse AMF (1/AMF, Fig. C1c), on the other hand, are in general much weaker than the SCD trends (approx. 3-4 times weaker) and do not follow the TCWV trend distribution. However, it occasionally happens that the relative inverse AMF trends either weaken or cancel the SCD trends (e.g. North America or Northeast Asia) or even strengthen them (e.g. around the Arabian peninsula). Overall, we conclude that the relative TCWV trends are mainly determined by the SCD trends, which consequently means that TCWV trends are mainly due to an increase in atmospheric water vapour concentration.

In addition to the trends of the SCD and AMF, we also analyze the trends of the AMF input parameters, i.e. the effective cloud fraction (CF), the cloud top height (CTH), and the surface albedo. The corresponding global distributions are depicted in Figure C2. Here, it is important to mention that the MPIC OMI TCWV data set only includes mostly clear-sky observations (i.e. CF < 20%), so the calculated trends of the cloud input parameters are very likely not representative for the actual cloud trends of the atmosphere. For CF (Fig. C2a) we obtain in general decreasing trends around $-0.1\,\%\,y^{-1}$ globally, except for the Indian subcontinent and some individual locations. For the input CTH (Fig. C2b) no clear trend pattern is observable, except for slight increasing trends over the tropical landmasses with values around $+0.03\,km\,y^{-1}$. As expected for the surface albedo (Fig. C2c) no trends are observable over ocean as a static monthly albedo map has been used here. Over land, however, strong varying

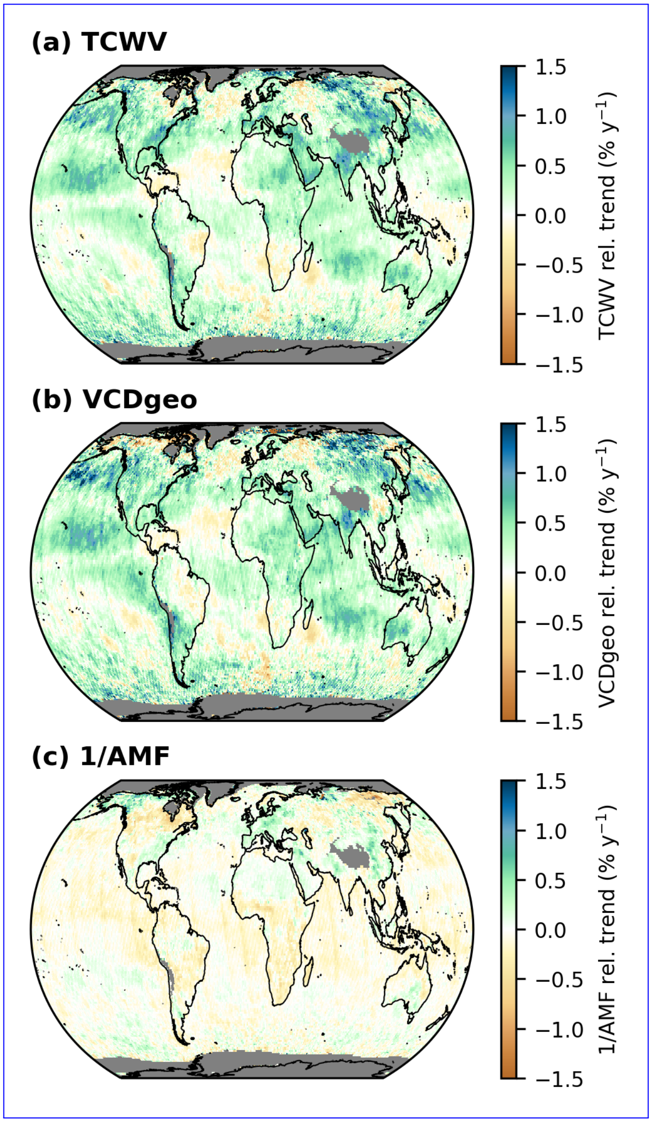

Figure C1. Global distributions of relative trends of the TCWV (a), geometrical vertical column density (VCDgeo, (b)) and the inverse of the air mass factor (1/AMF, (c)) for the time period January 2005 to December 2020. Grid cells for which no trend has been calculated are coloured grey.

trends can be found in the high latitudes of the Northern hemisphere with absolute values higher than 0.2 % y^{-1}. Nevertheless, these strong albedo trends in the Northern hemisphere are typically not significant.

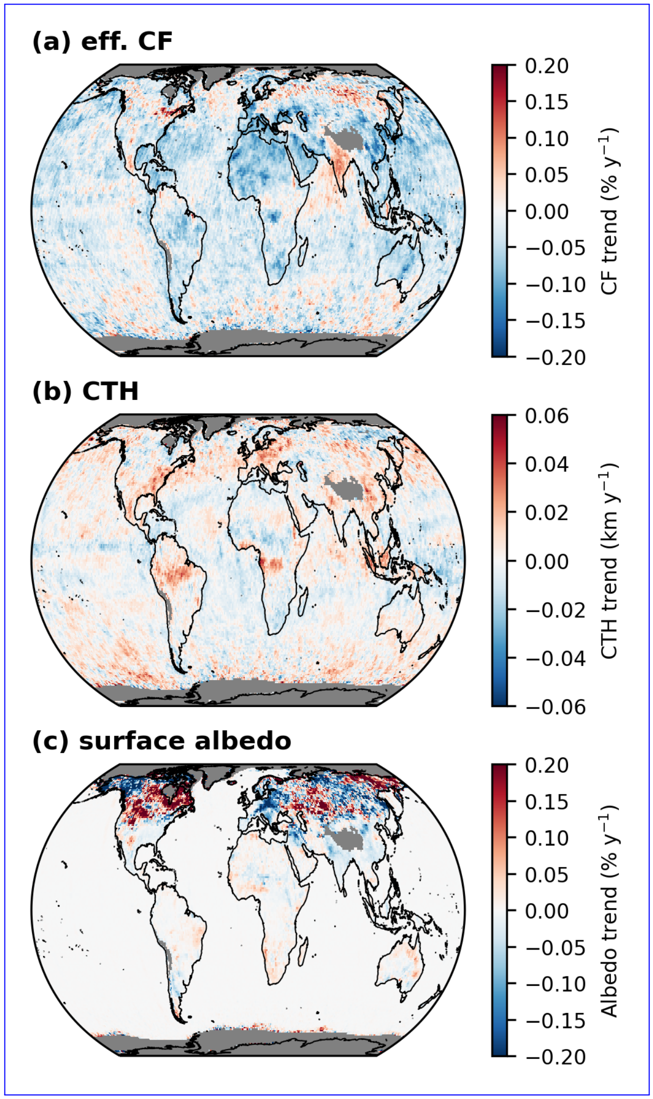

Figure C2. Absolute trends of the retrieval input parameters for the calculation of the airmass factor for the time period January 2005 to December 2020: (a) effective cloud fraction; (b) cloud top height; (c) surface albedo. Grid cells for which no trend has been calculated are coloured grey.

Appendix D: Intercomparison to trends from other studies

In the following we compare our results of relative TCWV trends for the time range 2005-2020 to trends presented in previous studies and investigate which TCWV trends are significant within the respective time range of the previous studies. It is particularly important to note that TCWV trends from different time periods have been investigated. For the sake of completeness, the global distributions of the absolute trends for the same data sets and time ranges are available in

Fig. S5 in the supplement.

Trenberth et al. (2005) analyzed trends from the RSS SSM/I data for the time period of 1988 to 2003. In general, the results of global relative TCWV trend distributions of both analyses share many similarities, however, in contrast to our results, they obtained a distinctive decrease in TCWV in the East Pacifictropics, where our analysis indicates a distinctive increase (compare While the patterns generally match quite well, the trends often have opposite signs: In our period (2005-2020) the trends are mainly positive, whereas in the period of this study (1988-2003) the trends are mainly negative. This is particularly visible in the Eastern Pacific. However, we were unable to identify any significant trends for this period (see Fig. 11 in their paper). Similar findings can also be obtained in the tropical Pacific and the East coast of Australia. In additionD1d). Overall, however, the trends of Trenberth et al. (2005) are overall approximately half as strong as our resultsin very good agreement with the trends we have determined for this period (compare Fig. 11 in their paper).

Mieruch et al. (2008) investigated TCWV trends from 1996 to 2006 using a TCWV data set created from measurements of GOME and SCIAMACHY using the AMC-DOAS method (Noël et al., 2004). Although as for the comparison to Trenberth et al. (2005)similarities can be found, many patterns In contrast to the comparison with Trenberth et al. (2005), especially these classified as significant, do not agree to our results. For instance, Mieruch et al. (2008) observe a distinctive relative TCWV decrease around the Arabian peninsula, howeveralmost no similarities are discernible either in the spatial patterns or in the strength of the trends. Overall, the spatial distribution is not as smooth as in the other periods studied and is distintively spottier. This is probably due to the fact that the period studied is quite short and that there was also a strong El Niño event in 1997/1998. Compared to the results in Mieruch et al. (2008) (Fig. 5 in their paper), our results suggest an increase in the TCWV content. Furthermore, Mieruch et al. (2008) found a decreasing trend in the tropical East Pacific (similar to Trenberth et al., 2005), where we observe a distinctive increase. Overall, it should be noted that the obtained relative for the same period find only few similarities, also in the significant trends. For example, the trends of Mieruch et al. (2008) are approximately 2 to 3 times larger than our results which is probably related to the relatively short time sometimes 4 to 6 times as high as ours for the same period.

More recently, Wang et al. (2016) also investigated TCWV trends for the time period from 1995 to 2011 for a TCWV data set combining measurements from radiosondes, GPS radio occultation, and microwave satellite instruments. As for the two aforementioned comparisonscomparison to Trenberth et al. (2005), our findings and the findings from Wang et al. (2016) share many similarities, but also several discrepancies: Wang et al. (2016) find a "sandwich" shape in the tropical and subtropical Pacific with positive trends in the region of the innertropical convergence zone bounded by two bands of negative trends. In contrast, the OMI TCWV trends also suggest a "sandwich" shape but with opposite signs to Wang et al. (2016), i.e. negative trends bounded by positive trends. Such opposite findings also occur over parts of the Indian subcontinent, the Arabian peninsula, and South America. However, for central Europe and parts of Asia good agreement for the trend results patterns is found.

For the comparisons of our results to the findings of Trenberth et al. (2005), Mieruch et al. (2008), and Wang et al. (2016) one explanation for the differences may be the different time periods of investigations (1988 to 2003, 1996 to 2006, and 1995 to 2011 vs. 2005 to 2020). Figures D1b-d c-h illustrate the relative TCWV trends derived from the ERA5 data set for the aforementioned time periods. Although only the time periods have been changed, clear differences can indeed be identified in both the distribution and the strength of the trends. Furthermore, these trend distributions agree very well with the results of the three previously mentioned studies. Nevertheless, different methodologies of observations or different methods for the trend calculation may also be a cause for the discrepancies. For instance, we explicitly account for the influence of ENSO by including the ONI and TNI index into our analysis scheme (see also Appendix ASect. 2.2 and Sect. 3.1), whereas Mieruch et al. (2008) explicitly filtered the time around the strongest ENSO signal.

Combining that the detected trends for ERA5 and the GOME-Evolution data set agree well to the findings from the OMI TCWV data set (see Sect. 3.2) but the comparisons to the results from other trend analysis studies show systematic differences, it is evident to not only compare trends for the same time periods but also to ensure that the same methodology for the trend analysis is used. As a lot of different methods exist for estimating trends in environmental data sets, it would be particularly interesting to evaluate which trend analysis scheme performs best and should be recommended for future studies. However, such an evaluation study is beyond the scope of this paper.

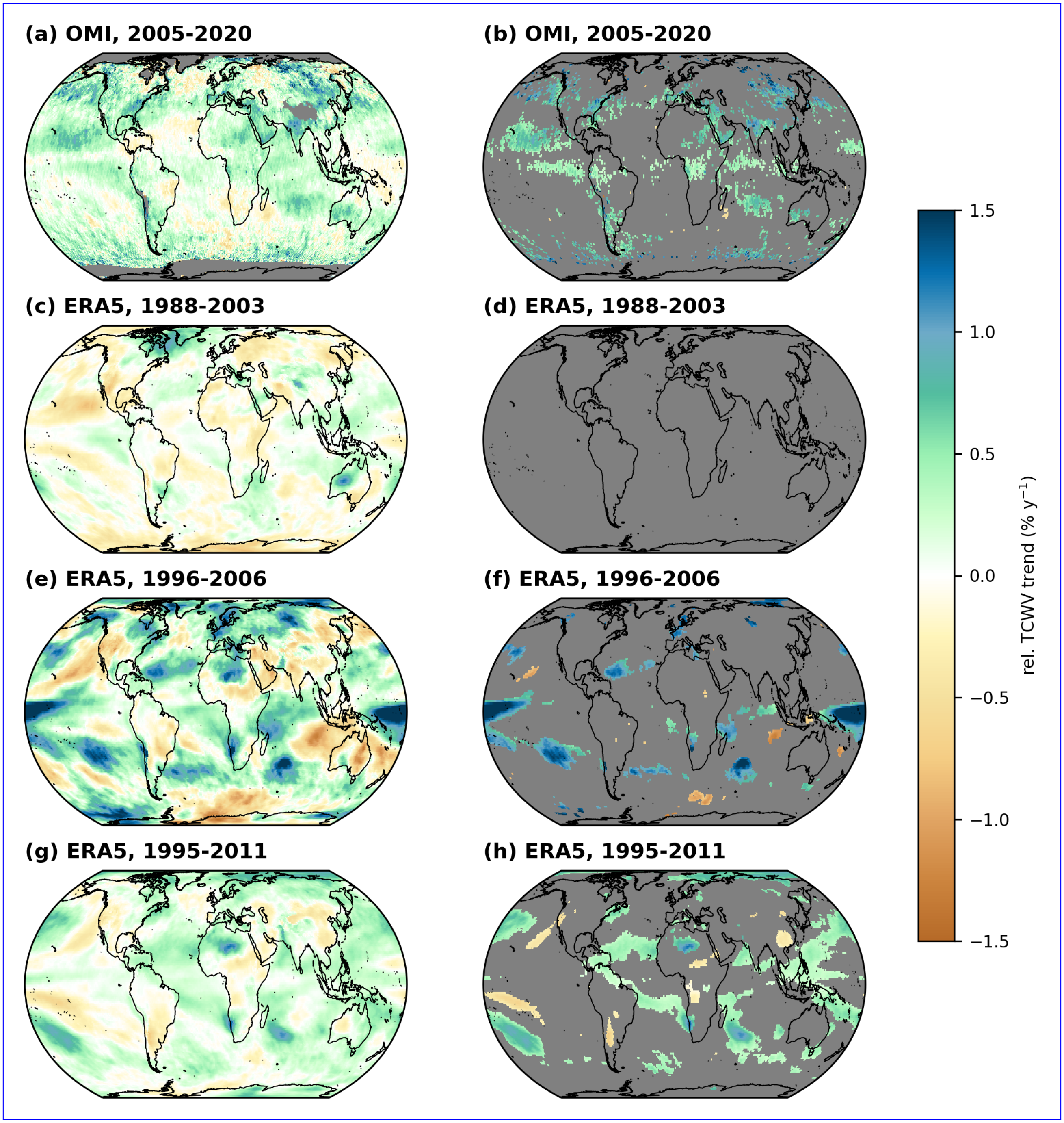

Figure D1. Global distributions of relative TCWV trends of OMI (2005-2020; Panel (a) & (b)) and ERA5 for different time periods: (bc) & (d) 1988-2003, ; (ce) & (f) 1996-2006, ; and (dg) & (h) 1995-2011. Panels in the left column illustrate all calculated trends and panels in the right column illustrate statistically significant trends after the application of a Z-test and a FDR test. Grid cells for which no valid trend has been calculated are coloured grey.

References

Allan, R. P., Soden, B. J., John, V. O., Ingram, W., and Good, P.: Current changes in tropical precipitation, Environmental Research Letters, 5, 025 205, https://doi.org/10.1088/1748-9326/5/2/025205, 2010.

Beirle, S., Lampel, J., Wang, Y., Mies, K., Dörner, S., Grossi, M., Loyola, D., Dehn, A., Danielczok, A., Schröder, M., and Wagner, T.: The ESA GOME-Evolution "Climate" water vapor product: a homogenized time series of H_2O columns from GOME, SCIAMACHY, and GOME-2, Earth System Science Data, 10, 449–468, https://doi.org/10.5194/essd-10-449-2018, 2018.

Benjamini, Y. and Hochberg, Y.: Controlling the False Discovery Rate: A Practical and Powerful Approach to Multiple Testing, Journal of the Royal Statistical Society. Series B (Methodological), 57, 289–300, http://www.jstor.org/stable/2346101, 1995.

Bennartz, R. and Fischer, J.: Retrieval of columnar water vapour over land from backscattered solar radiation using the Medium Resolution Imaging Spectrometer, Remote Sensing of Environment, 78, 274–283, https://doi.org/10.1016/S0034-4257(01)00218-8, 2001.

Borger, C., Beirle, S., Dörner, S., Sihler, H., and Wagner, T.: Total column water vapour retrieval from S-5P/TROPOMI in the visible blue spectral range, Atmospheric Measurement Techniques, 13, 2751–2783, https://doi.org/10.5194/amt-13-2751-2020, 2020.

Borger, C., Beirle, S., and Wagner, T.: A 16-year global climate data record of total column water vapour generated from OMI observations in the visible blue spectral range, Earth System Science Data Discussions, 2021, 1–25, https://doi.org/10.5194/essd-2021-319, 2021a.

Borger, C., Beirle, S., and Wagner, T.: MPIC OMI Total Column Water Vapour (TCWV) Climate Data Record, https://doi.org/10.5281/zenodo.5776718, 2021b.

Borger, C., Beirle, S., and Wagner, T.: Detecting Hadley cell expansion directly from satellite observations of water vapour, to be submitted, 2022.

Bourdin, S., Kluft, L., and Stevens, B.: Dependence of Climate Sensitivity on the Given Distribution of Relative Humidity, Geophysical Research Letters, 48, e2021GL092 462, https://doi.org/https://doi.org/10.1029/2021GL092462, e2021GL092462 2021GL092462, 2021.

Bretherton, C. S., Peters, M. E., and Back, L. E.: Relationships between Water Vapor Path and Precipitation over the Tropical Oceans, Journal of Climate, 17, 1517 – 1528, https://doi.org/10.1175/1520-0442(2004)017<1517:RBWVPA>2.0.CO;2, 2004.

Byrne, M. P. and O'Gorman, P. A.: Trends in continental temperature and humidity directly linked to ocean warming, Proceedings of the National Academy of Sciences, 115, 4863–4868, https://doi.org/10.1073/pnas.1722312115, 2018.

Cheng, L., Trenberth, K. E., Gruber, N., Abraham, J. P., Fasullo, J. T., Li, G., Mann, M. E., Zhao, X., and Zhu, J.: Improved Estimates of Changes in Upper Ocean Salinity and the Hydrological Cycle, Journal of Climate, 33, 10 357 – 10 381, https://doi.org/10.1175/JCLI-D-20-0366.1, 2020.

Chiang, J. C. H. and Vimont, D. J.: Analogous Pacific and Atlantic Meridional Modes of Tropical Atmosphere–Ocean Variability, Journal of Climate, 17, 4143 – 4158, https://doi.org/10.1175/JCLI4953.1, 2004.

Chou, C., Neelin, J. D., Chen, C.-A., and Tu, J.-Y.: Evaluating the "rich-get-richer" mechanism in tropical precipitation change under global warming, Journal of Climate, 22, 1982–2005, https://doi.org/10.1175/2008JCLI2471.1, 2009.

Chou, C., Chiang, J. C. H., Lan, C.-W., Chung, C.-H., Liao, Y.-C., and Lee, C.-J.: Increase in the range between wet and dry season precipitation, Nature Geoscience, 6, 263–267, https://doi.org/10.1038/ngeo1744, 2013.

Dai, A.: Recent climatology, variability, and trends in global surface humidity, Journal of Climate, 19, 3589–3606, https://doi.org/10.1175/JCLI3816.1, 2006.

Danielson, J. J. and Gesch, D. B.: Global multi-resolution terrain elevation data 2010 (GMTED2010), Tech. rep., https://doi.org/10.3133/ofr20111073, report, 2011.

Dunn, R. J. H., Willett, K. M., Ciavarella, A., and Stott, P. A.: Comparison of land surface humidity between observations and CMIP5 models, Earth System Dynamics, 8, 719–747, https://doi.org/10.5194/esd-8-719-2017, 2017.

Fasullo, J.: A mechanism for land–ocean contrasts in global monsoon trends in a warming climate, Climate Dynamics, 39, 1137–1147, https://doi.org/10.1007/s00382-011-1270-3, 2012.

Foster, G. and Rahmstorf, S.: Global temperature evolution 1979–2010, Environmental Research Letters, 6, 044 022, https://doi.org/10.1088/1748-9326/6/4/044022, 2011.

Gao, B.-C. and Kaufman, Y. J.: Water vapor retrievals using Moderate Resolution Imaging Spectroradiometer (MODIS) near-infrared channels, Journal of Geophysical Research: Atmospheres, 108, https://doi.org/10.1029/2002JD003023, 2003.

Gimeno, L., Eiras-Barca, J., Durán-Quesada, A. M., Dominguez, F., van der Ent, R., Sodemann, H., Sánchez-Murillo, R., Nieto, R., and Kirchner, J. W.: The residence time of water vapour in the atmosphere, Nature Reviews Earth & Environment, 2, 558–569, https://doi.org/10.1038/s43017-021-00181-9, 2021.

Greve, P., Orlowsky, B., Mueller, B., Sheffield, J., Reichstein, M., and Seneviratne, S. I.: Global assessment of trends in wetting and drying over land, Nature Geoscience, 7, 716–721, https://doi.org/10.1038/ngeo2247, 2014.

Grossi, M., Valks, P., Loyola, D., Aberle, B., Slijkhuis, S., Wagner, T., Beirle, S., and Lang, R.: Total column water vapour measurements from GOME-2 MetOp-A and MetOp-B, Atmospheric Measurement Techniques, 8, 1111–1133, https://doi.org/10.5194/amt-8-1111-2015, 2015.

Held, I. M. and Soden, B. J.: Water Vapor Feedback and Global Warming, Annual Review of Energy and the Environment, 25, 441–475, https://doi.org/10.1146/annurev.energy.25.1.441, 2000.

Held, I. M. and Soden, B. J.: Robust Responses of the Hydrological Cycle to Global Warming, Journal of Climate, 19, 5686 – 5699, https://doi.org/10.1175/JCLI3990.1, 2006.

Hersbach, H., Bell, B., Berrisford, P., Biavati, G., Horányi, A., Muñoz Sabater, J., Nicolas, J., Peubey, C., Radu, R., Rozum, I., Schepers, D., Simmons, A., Soci, C., Dee, D., and Thépaut, J.-N.: ERA5 monthly averaged data on single levels from 1979 to present, Copernicus Climate Change Service (C3S) Climate Data Store (CDS), https://doi.org/10.24381/cds.f17050d7, (Accessed on: 2021-07-01), 2019.

Hersbach, H., Bell, B., Berrisford, P., Hirahara, S., Horányi, A., Muñoz-Sabater, J., Nicolas, J., Peubey, C., Radu, R., Schepers, D., Simmons, A., Soci, C., Abdalla, S., Abellan, X., Balsamo, G., Bechtold, P., Biavati, G., Bidlot, J., Bonavita, M., De Chiara, G., Dahlgren, P., Dee, D., Diamantakis, M., Dragani, R., Flemming, J., Forbes, R., Fuentes, M., Geer, A., Haimberger, L., Healy, S., Hogan, R. J., Hólm, E., Janisková, M., Keeley, S., Laloyaux, P., Lopez, P., Lupu, C., Radnoti, G., de Rosnay, P., Rozum, I., Vamborg, F., Villaume, S., and Thépaut, J.-N.: The ERA5 global reanalysis, Quarterly Journal of the Royal Meteorological Society, 146, 1999–2049, https://doi.org/10.1002/qj.3803, 2020.

Huffman, G., Behrangi, A., Bolvin, D., and Nelkin, E.: GPCP Version 3.1 Satellite-Gauge (SG) Combined Precipitation Data Set, NASA GES DISC, https://doi.org/10.5067/DBVUO4KQHXTK, 2020.

Kiehl, J. T. and Trenberth, K. E.: Earth's Annual Global Mean Energy Budget., Bulletin of the American Meteorological Society, 78, 197–197, https://doi.org/10.1175/1520-0477(1997)078<0197:EAGMEB>2.0.CO;2, 1997.

Kursinski, E. R., Hajj, G. A., Schofield, J. T., Linfield, R. P., and Hardy, K. R.: Observing Earth's atmosphere with radio occultation measurements using the Global Positioning System, Journal of Geophysical Research: Atmospheres, 102, 23 429–23 465, https://doi.org/10.1029/97JD01569, 1997.

Lang, R., Williams, J. E., van der Zande, W. J., and Maurellis, A. N.: Application of the Spectral Structure Parameterization technique: retrieval of total water vapor columns from GOME, Atmospheric Chemistry and Physics, 3, 145–160, https://doi.org/10.5194/acp-3-145-2003, 2003.

Levelt, P. F., van den Oord, G. H., Dobber, M. R., Malkki, A., Visser, H., de Vries, J., Stammes, P., Lundell, J. O., and Saari, H.: The ozone monitoring instrument, IEEE Transactions on Geoscience and Remote Sensing, 44, 1093–1101, https://doi.org/10.1109/TGRS.2006.872333, 2006.

Levelt, P. F., Joiner, J., Tamminen, J., Veefkind, J. P., Bhartia, P. K., Stein Zweers, D. C., Duncan, B. N., Streets, D. G., Eskes, H., van der A, R., McLinden, C., Fioletov, V., Carn, S., de Laat, J., DeLand, M., Marchenko, S., McPeters, R., Ziemke, J., Fu, D., Liu, X., Pickering, K., Apituley, A., González Abad, G., Arola, A., Boersma, F., Chan Miller, C., Chance, K., de Graaf, M., Hakkarainen, J., Hassinen, S., Ialongo, I., Kleipool, Q., Krotkov, N., Li, C., Lamsal, L., Newman, P., Nowlan, C., Suleiman, R., Tilstra, L. G., Torres, O., Wang, H., and Wargan, K.: The Ozone Monitoring Instrument: overview of 14 years in space, Atmospheric Chemistry and Physics, 18, 5699–5745, https://doi.org/10.5194/acp-18-5699-2018, 2018.

Mears, C. A., Wang, J., Smith, D., and Wentz, F. J.: Intercomparison of total precipitable water measurements made by satellite-borne microwave radiometers and ground-based GPS instruments, Journal of Geophysical Research: Atmospheres, 120, 2492–2504, https://doi.org/10.1002/2014JD022694, 2015.

Mieruch, S., Noël, S., Bovensmann, H., and Burrows, J. P.: Analysis of global water vapour trends from satellite measurements in the visible spectral range, Atmospheric Chemistry and Physics, 8, 491–504, https://doi.org/10.5194/acp-8-491-2008, 2008.

Morice, C. P., Kennedy, J. J., Rayner, N. A., Winn, J. P., Hogan, E., Killick, R. E., Dunn, R. J. H., Osborn, T. J., Jones, P. D., and Simpson, I. R.: An Updated Assessment of Near-Surface Temperature Change From 1850: The HadCRUT5 Data Set, Journal of Geophysical Research: Atmospheres, 126, e2019JD032 361, https://doi.org/10.1029/2019JD032361, e2019JD032361 2019JD032361, 2021.

Noël, S., Buchwitz, M., Bovensmann, H., Hoogen, R., and Burrows, J. P.: Atmospheric water vapor amounts retrieved from GOME satellite data, Geophysical Research Letters, 26, 1841–1844, https://doi.org/10.1029/1999GL900437, 1999.

Noël, S., Buchwitz, M., and Burrows, J. P.: First retrieval of global water vapour column amounts from SCIAMACHY measurements, Atmospheric Chemistry and Physics, 4, 111–125, https://doi.org/10.5194/acp-4-111-2004, 2004.

O'Gorman, P. A. and Muller, C. J.: How closely do changes in surface and column water vapor follow Clausius-Clapeyron scaling in climate change simulations?, Environmental Research Letters, 5, 025 207, https://doi.org/10.1088/1748-9326/5/2/025207, 2010.

Platt, U. and Stutz, J.: Differential Optical Absorption Spectroscopy: Principles and Applications, Physics of Earth and Space Environments, Springer Berlin Heidelberg, https://doi.org/10.1007/978-3-540-75776-4, 2008.

Prais, S. J. and Winsten, C. B.: Trend Estimators and Serial Correlation, Cowles Commission Discussion Paper, 383, https://cowles.yale.edu/sites/default/files/files/pub/cdp/s-0383.pdf, unpublished, 1954.

Prat, O. P., Nelson, B. R., Nickl, E., and Leeper, R. D.: Global Evaluation of Gridded Satellite Precipitation Products from the NOAA Climate Data Record Program, Journal of Hydrometeorology, 22, 2291 – 2310, https://doi.org/10.1175/JHM-D-20-0246.1, 2021.

Randall, D. A., Wood, R. A., Bony, S., Colman, R., Fichefet, T., Fyfe, J., Kattsov, V., Pitman, A., Shukla, J., Srinivasan, J., et al.: Climate models and their evaluation, in: Climate change 2007: The physical science basis. Contribution of Working Group I to the Fourth Assessment Report of the IPCC (FAR), pp. 589–662, Cambridge University Press, 2007.

Rehfeld, K., Marwan, N., Heitzig, J., and Kurths, J.: Comparison of correlation analysis techniques for irregularly sampled time series, Nonlinear Processes in Geophysics, 18, 389–404, https://doi.org/10.5194/npg-18-389-2011, 2011.

Rohde, R. A. and Hausfather, Z.: The Berkeley Earth Land/Ocean Temperature Record, Earth System Science Data, 12, 3469–3479, https://doi.org/10.5194/essd-12-3469-2020, 2020.

Rosenkranz, P. W.: Retrieval of temperature and moisture profiles from AMSU-A and AMSU-B measurements, IEEE Transactions on Geoscience and Remote Sensing, 39, 2429–2435, https://doi.org/10.1109/36.964979, 2001.

Rushley, S. S., Kim, D., Bretherton, C. S., and Ahn, M.-S.: Reexamining the Nonlinear Moisture-Precipitation Relationship Over the Tropical Oceans, Geophysical Research Letters, 45, 1133–1140, https://doi.org/10.1002/2017GL076296, 2018.

Schröder, M., Lockhoff, M., Forsythe, J. M., Cronk, H. Q., Haar, T. H. V., and Bennartz, R.: The GEWEX Water Vapor Assessment: Results from Intercomparison, Trend, and Homogeneity Analysis of Total Column Water Vapor, Journal of Applied Meteorology and Climatology, 55, 1633 – 1649, https://doi.org/10.1175/JAMC-D-15-0304.1, 2016.

Sherwood, S. and Fu, Q.: A Drier Future?, Science, 343, 737–739, https://doi.org/10.1126/science.1247620, 2014.

Simmons, A. J., Willett, K. M., Jones, P. D., Thorne, P. W., and Dee, D. P.: Low-frequency variations in surface atmospheric humidity, temperature, and precipitation: Inferences from reanalyses and monthly gridded observational data sets, Journal of Geophysical Research: Atmospheres, 115, https://doi.org/https://doi.org/10.1029/2009JD012442, 2010.

Singh, H. K. A., Bitz, C. M., Donohoe, A., Nusbaumer, J., and Noone, D. C.: A Mathematical Framework for Analysis of Water Tracers. Part II: Understanding Large-Scale Perturbations in the Hydrological Cycle due to CO2 Doubling, Journal of Climate, 29, 6765 – 6782, https://doi.org/10.1175/JCLI-D-16-0293.1, 2016.

Sodemann, H.: Beyond Turnover Time: Constraining the Lifetime Distribution of Water Vapor from Simple and Complex Approaches, Journal of the Atmospheric Sciences, 77, 413 – 433, https://doi.org/10.1175/JAS-D-18-0336.1, 2020.

Staten, P. W., Lu, J., Grise, K. M., Davis, S. M., and Birner, T.: Re-examining tropical expansion, Nature Climate Change, 8, 768–775, https://doi.org/10.1038/s41558-018-0246-2, 2018.

Susskind, J., Barnet, C., and Blaisdell, J.: Retrieval of atmospheric and surface parameters from AIRS/AMSU/HSB data in the presence of clouds, IEEE Transactions on Geoscience and Remote Sensing, 41, 390–409, https://doi.org/10.1109/TGRS.2002.808236, 2003.

Trenberth, K. E.: Atmospheric Moisture Residence Times and Cycling: Implications for Rainfall Rates and Climate Change, Climatic Change, 39, 667–694, https://doi.org/10.1023/A:1005319109110, 1998.

Trenberth, K. E.: Changes in precipitation with climate change, Climate Research, 47, 123–138, https://doi.org/10.3354/cr00953, 2011.

Trenberth, K. E. and Shea, D. J.: Relationships between precipitation and surface temperature, Geophysical Research Letters, 32, https://doi.org/10.1029/2005GL022760, 2005.

Trenberth, K. E. and Stepaniak, D. P.: Indices of El Niño Evolution, Journal of Climate, 14, 1697 – 1701, https://doi.org/10.1175/1520-0442(2001)014<1697:LIOENO>2.0.CO;2, 2001.

Trenberth, K. E., Fasullo, J., and Smith, L.: Trends and variability in column-integrated atmospheric water vapor, Climate Dynamics, 24, 741–758, https://doi.org/10.1007/s00382-005-0017-4, 2005.

van der Ent, R. J. and Tuinenburg, O. A.: The residence time of water in the atmosphere revisited, Hydrology and Earth System Sciences, 21, 779–790, https://doi.org/10.5194/hess-21-779-2017, 2017.

von Storch, H.: Misuses of Statistical Analysis in Climate Research, in: Analysis of Climate Variability, edited by von Storch, H. and Navarra, A., pp. 11–26, Springer Berlin Heidelberg, Berlin, Heidelberg, 1999.

Wagner, T., Heland, J., Zöger, M., and Platt, U.: A fast H_2O total column density product from GOME - Validation with in-situ aircraft measurements, Atmospheric Chemistry and Physics, 3, 651–663, https://doi.org/10.5194/acp-3-651-2003, 2003.

Wagner, T., Beirle, S., Grzegorski, M., and Platt, U.: Global trends (1996–2003) of total column precipitable water observed by Global Ozone Monitoring Experiment (GOME) on ERS-2 and their relation to near-surface temperature, Journal of Geophysical Research: Atmospheres, 111, https://doi.org/10.1029/2005JD006523, 2006.

Wagner, T., Beirle, S., Deutschmann, T., Grzegorski, M., and Platt, U.: Satellite monitoring of different vegetation types by differential optical absorption spectroscopy (DOAS) in the red spectral range, Atmospheric Chemistry and Physics, 7, 69–79, https://doi.org/10.5194/acp-7-69-2007, 2007.

Wagner, T., Beirle, S., Dörner, S., Borger, C., and Van Malderen, R.: Identification of atmospheric and oceanic teleconnection patterns in a 20-year global data set of the atmospheric water vapour column measured from satellites in the visible spectral range, Atmospheric Chemistry and Physics, 21, 5315–5353, https://doi.org/10.5194/acp-21-5315-2021, 2021.

Wang, J., Dai, A., and Mears, C.: Global Water Vapor Trend from 1988 to 2011 and Its Diurnal Asymmetry Based on GPS, Radiosonde, and Microwave Satellite Measurements, Journal of Climate, 29, 5205 – 5222, https://doi.org/10.1175/JCLI-D-15-0485.1, 2016.

Weatherhead, E. C., Reinsel, G. C., Tiao, G. C., Meng, X.-L., Choi, D., Cheang, W.-K., Keller, T., DeLuisi, J., Wuebbles, D. J., Kerr, J. B., Miller, A. J., Oltmans, S. J., and Frederick, J. E.: Factors affecting the detection of trends: Statistical considerations and applications to environmental data, Journal of Geophysical Research: Atmospheres, 103, 17 149–17 161, https://doi.org/10.1029/98JD00995, 1998.

Wentz, F. J.: A 17-Yr Climate Record of Environmental Parameters Derived from the Tropical Rainfall Measuring Mission (TRMM) Microwave Imager, Journal of Climate, 28, 6882 – 6902, https://doi.org/10.1175/JCLI-D-15-0155.1, 2015.

Wilks, D. S.: On "Field Significance" and the False Discovery Rate, Journal of Applied Meteorology and Climatology, 45, 1181 – 1189, https://doi.org/10.1175/JAM2404.1, 2006.

Wilks, D. S.: Statistical Methods in the Atmospheric Sciences, vol. 100 of *International Geophysics*, Elsevier Academic Press, Amsterdam, 3 edn., https://www.sciencedirect.com/bookseries/international-geophysics/vol/100/suppl/C, 2011.

Wilks, D. S.: "The Stippling Shows Statistically Significant Grid Points": How Research Results are Routinely Overstated and Overinterpreted, and What to Do about It, Bulletin of the American Meteorological Society, 97, 2263 – 2273, https://doi.org/10.1175/BAMS-D-15-00267.1, 2016.

Willett, K. M., Dunn, R. J. H., Thorne, P. W., Bell, S., de Podesta, M., Parker, D. E., Jones, P. D., and Williams Jr., C. N.: HadISDH land surface multi-variable humidity and temperature record for climate monitoring, Climate of the Past, 10, 1983–2006, https://doi.org/10.5194/cp-10-1983-2014, 2014.

Willett, K. M., Dunn, R. J. H., Kennedy, J. J., and Berry, D. I.: Development of the HadISDH.marine humidity climate monitoring dataset, Earth System Science Data, 12, 2853–2880, https://doi.org/10.5194/essd-12-2853-2020, 2020.